

Chapter 15

Mass Loss Processes in Titan's Upper Atmosphere

R.E. Johnson, O.J. Tucker, M. Michael, E.C. Sittler, H.T. Smith, D.T. Young, and J.H. Waite

Abstract Although Titan's atmospheric column density is about ten times that of the Earth's, its measured $^{15}\text{N}/^{14}\text{N}$ ratio suggests that considerable escape has occurred or that Titan's original material had a ratio closer to that of cometary materials. A number of active escape processes have been proposed: thermal escape, chemical-induced escape, slow hydrodynamic escape, pick-up ion loss, ionospheric outflow and plasma-ion-induced atmospheric sputtering. These loss processes and relevant simulations are reviewed in light of recent Cassini data.

Analysis of Cassini data collected in Titan's thermosphere and corona indicate that thermal loss of hydrogen occurs at a rate comparable to pre-Cassini estimates. This escape of hydrogen is accompanied by a significant loss of methane due to formation and precipitation of hydrocarbons ($\sim 2 \times 10^{29}$ amu/s). However, there is much less agreement on the rates for the escape of methane and nitrogen. Recent estimates, $\sim 0.3\text{--}5 \times 10^{28}$ amu/s, are much larger than the pre-Cassini estimates and also much larger than the measured ion loss rates ($\sim 1\text{--}5 \times 10^{26}$ amu/s). If the largest heavy molecule escape rates are assumed, a significant fraction of the present atmosphere would have been lost to space in 4 Gyr. Because understanding the nature of the active escape processes is critical, a number of data sets were used to model the methane and nitrogen escape rates. The solar heating/cooling rate and the nitrogen density profile vs altitude were used in a fluid dynamic model to extract an average net

upward flux below the exobase; the altitude dependence of the diffusion of methane through nitrogen was described below the exobase allowing for upward flow and escape; the coronal structure above the exobase was simulated by plasma and photon-induced hot particle production; and measurements of the emission from excited-dissociation products were used to estimate escape. In the latter two models, hot recoils from photochemistry or plasma-ion-induced heating lead to escape, whereas in the first two models heat conduction from below was assumed to enhance Jeans escape, a process referred to as slow hydrodynamic escape. These models are compared to each other and to recent simulations of Titan's exobase region. It is found that these simulations are inconsistent with the slow hydrodynamic escape model and that the composition of the magnetospheric plasma at Titan's orbit is inconsistent with the largest carbon loss rates suggested.

15.1 Introduction

Titan is unique among outer solar system satellites in that it has an atmosphere with a column density about ten times that of Earth and an atmospheric mass to solid ratio comparable to that of Venus. Titan's atmosphere is not only thick, but is also extended and consists of over 95% N_2 , about 2–3% CH_4 with some H_2 and other minor species. If such an atmosphere had been present on Io, Europa or Ganymede in an earlier epoch, it would have been removed by plasma trapped in the Jovian magnetosphere (Johnson 2004). Therefore, the use of Cassini spacecraft data to understand the persistence of Titan's atmosphere and to describe its present mass loss rate provides an important end point for understanding the erosion of atmospheres on other planets and satellites. It is also important for describing Titan's role in populating Saturn's magnetosphere with neutrals and plasma. The emphasis in this chapter is atmospheric escape, but mass loss to the surface will also be discussed because it is related. Loss processes are often given as a molecular flux, but to compare the relative importance of the escape processes, global average mass loss rates will also be considered.

R.E. Johnson and O.J. Tucker (✉)
University of Virginia, Charlottesville, VA, 22904, USA
Physics Department, NYU, NY, 10003, USA
email: rej@virginia.edu

M. Michael
Department Civil Engineering, Indian Institute of Technology,
Kanpur, India

E.C. Sittler
GSFC, Greenbelt, MD, USA

H.T. Smith
JHUAPL, Laurel, MD, USA

D.T. Young and J.H. Waite
SwRI, San Antonio, TX, USA

Prior to Cassini's arrival at Saturn, modeling based on Voyager data indicated that the hydrogen escape rate was large ($\sim 1\text{--}3 \times 10^{28}$ amu/s) (e.g., Lebonnois et al. 2003) consistent with a large loss rate for methane by precipitation as hydrocarbons, $\sim 10\text{--}30 \times 10^{28}$ amu/s (e.g., Wilson and Atreya 2004). However, the rates for carbon and nitrogen escape to space were estimated to be relatively small ($\sim 0.05 \times 10^{28}$ amu/s) and dominated by atmospheric sputtering (Shematovich et al. 2003). Recent analysis of the structure of Titan's thermosphere and corona attained from Cassini data have led to substantially larger estimates of the escape rate for these heavier species ($0.3\text{--}5 \times 10^{28}$ amu/s). At the largest escape rates suggested, a mass that is about the size of the present atmosphere would have been lost to space in 4 Gyr. Although this atmospheric loss rate is still an order of magnitude smaller than the carbon precipitation rate, evaluating the proposed escape processes is critical for understanding the evolution of Titan's atmosphere.

Atoms and molecules can be lost from an atmosphere both as ions and neutrals as indicated in Fig. 15.1. A number of active escape processes have been proposed: thermal escape (Cui et al. 2008), chemically-induced escape (DeLaHaye et al. 2007b), slow hydrodynamic escape (Strobel 2008a, 2009; Yelle et al. 2008), pick-up ion loss and ionospheric outflow (Ledvina et al. 2005; Wahlund et al. 2005; Sillanpaa et al. 2006; Ma et al. 2006; Hartle et al. 2006a, b; Coates et al. 2007) and plasma-induced atmospheric sputtering (Shematovich et al. 2003; Michael et al. 2005a; DeLaHaye 2007a).

The mass loss rate due to pick-up ion formation and sweeping combined with ionospheric outflow is highly variable and of the order of $\sim 10^{25}$ amu/s (Wahlund et al. 2005; Hartle et al. 2006a, b). Globally averaged loss rates for

neutrals have been estimated using 1D models of Cassini data. The altitude dependence of the H_2 density was used to obtain a hydrogen loss rate of $\sim 1.6 \times 10^{28}$ amu/s (Cui et al. 2008). Bell et al. (2009) recently obtained a similar result. Hydrogen loss implies that methane is lost by precipitation ($\sim 2 \times 10^{29}$ amu/s using the largest rate) starting at relatively high altitudes in Titan's atmosphere (Chapter 8; Mandt et al. 2009). Three different 1D models were used to estimate a heavy molecule loss rate: $\sim 0.3\text{--}5 \times 10^{28}$ amu/s. The solar heating rate was used in a fluid dynamic model to extract an average net upward flux below the exobase (Strobel 2008a, 2009); the diffusion of methane through nitrogen was described below the exobase allowing for escape (Yelle et al. 2008); and the coronal structure above the exobase was simulated by presuming the observed density profiles were due to solar- and plasma-induced hot particle production (DeLaHaye et al. 2007a). In the latter, the hot recoils from photochemistry and the incident plasma produce the coronal structure. In the former models, the upward flow is assumed to be driven by heat conduction from below and referred to as slow hydrodynamic escape (Strobel 2008a). In this chapter these models are compared to each other and to recent simulations of the exobase region. The simulations and preliminary estimates of the composition of the magnetospheric plasma at Titan's orbit appear to be inconsistent with the largest methane escape rates suggested. However, because of the changing relationship between the solar and plasma illuminations (Fig. 15.1) and the plasma variability (Chapter 16), there is considerable work to be done in order to understand the extensive Cassini data set. Although the situation at Titan differs from that at Mars and Venus where the plasma and sunlight both come from, roughly, the same direction, the changing encounter geometries

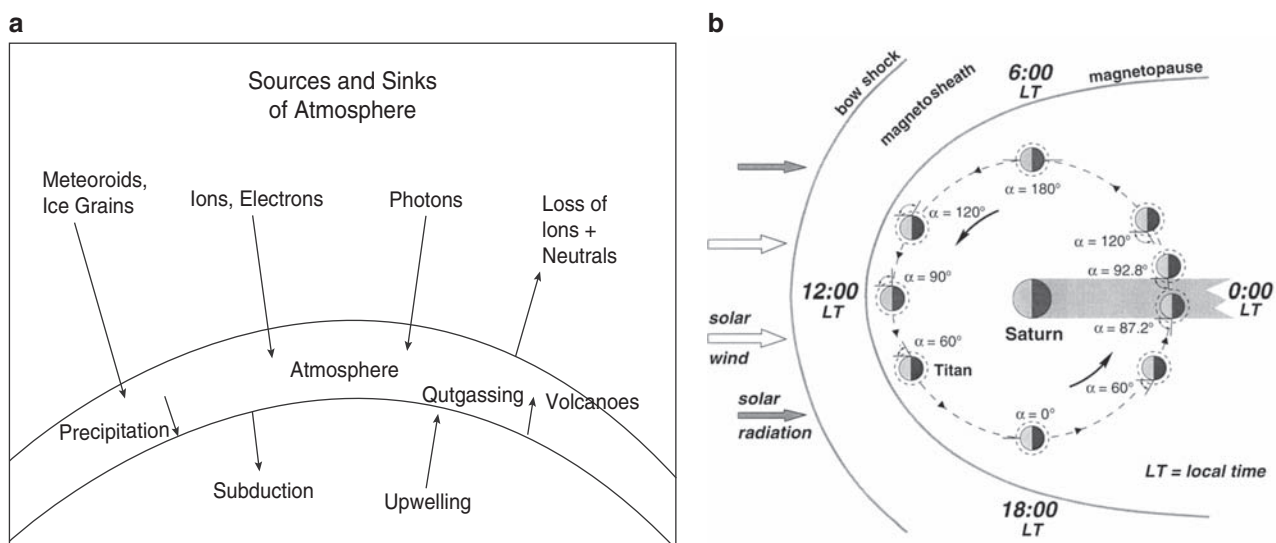


Fig. 15.1 Left panel: atmospheric sources and sinks: emphasis in this chapter is on mass loss rates due to escape and precipitation. Right panel: change in relationship between solar and plasma flux (see also Chapter 16).

at Titan can provide an opportunity to unravel the plasma- and solar-induced effects.

Below, each proposed active escape process is briefly described, followed by a short review of the pre-Cassini estimates of atmospheric mass loss, then a review of the recent mass loss calculations based on Cassini data and a summary.

15.2 Atmospheric Escape

Since the atmosphere decreases in density with increasing distance from the center of a planetary body, an altitude is eventually reached above which molecules that are moving radially outward can travel planetary scale distances with a very small probability of making a collision. At such altitudes a molecule can escape to space if its kinetic energy is greater than its gravitational binding energy and its radial velocity is outward. This region of the atmosphere is called the exosphere or the planetary corona. The lower boundary for this region, called the exobase, is defined as that altitude where the ratio of the mean free path for collisions, l_c , to the atmospheric scale height, H , is about one. In rarefied gas dynamics this ratio is the Knudsen number: $\text{Kn} = l_c/H$. It defines the transition region between where a gas that is dominated by collisions and can be modeled as a fluid, $\text{Kn} < 1$, gradually changes to a gas that should be modeled stochastically, $\text{Kn} \geq 0.1$, with the nominal exobase given by $\text{Kn} \sim 1$.

Simulations have shown that the appropriate l_c is the mean free path prior to a significant momentum transfer collision (e.g., Johnson 1994). Using realistic potentials such simulations also show that $l_c \sim 2/(n\sigma_d)$ where σ_d is momentum transfer (diffusion) cross section of the escaping particle averaged over the composition of the background gas (Johnson 1990, 1994; Johnson et al. 2000). Hot atoms and molecules escape from depths well below the nominal exobase, as seen in Fig. 15.2. Therefore, the often used Chamberlain model, in which escape occurs from the exobase, is a rough approximation. Assuming hot particles move upward at random angles, the average escape depth, given as a column density is $N(r_{\text{exo}}) \approx 1.3/\sigma_d$, can be used to determine the radial position of the nominal exobase, r_{exo} (e.g., Johnson 1994; Johnson et al. 2008). This column density should be averaged over the composition, which changes with altitude, and the energy distribution of escaping molecules. It is also evident that the exobase level is different for different escaping molecules in the same atmosphere. Since the ion-neutral momentum transfer cross section, often dominated by charge exchange, is about an order of magnitude larger than the neutral-neutral cross section, effects of the plasma ions on Titan's neutral atmosphere extend well above the nominal exobase.

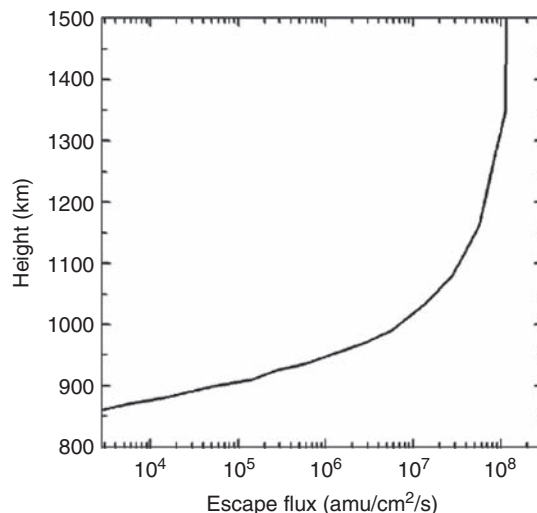


Fig. 15.2 Average upward integrated mass flux for molecular escape due to photochemistry in Titan's upper atmosphere from Shematovich et al. (2003): $\sim 1.2 \times 10^8$ amu/cm²/s at the exobase ~ 1500 km ($\text{Kn} \sim 1$); if the escape occurs over the hemisphere (exobase area $\sim 1.0 \times 10^{18}$ cm²) the loss rate is $\sim 1.2 \times 10^{26}$ amu/s. This figure shows the depth of origin of the escaping hot recoils, indicating the transition region, where the fluid approximation gives way to the kinetic regime, occurs well below the nominal exobase.

15.2.1 Thermal Escape

Planetary and satellite atmospheres confined by gravity are often characterized by the Jeans parameter, λ , which is the ratio of the gravitational energy to the thermal energy: $\lambda = [(GMm/r_{\text{exo}})/kT] = r_{\text{exo}}/H_{\text{exo}}$, where H_{exo} is the atmospheric scale height at the exobase and r_{exo} is the exobase radius. Since $H_{\text{exo}} = r_{\text{exo}}/\lambda$, with increasing λ the atmosphere becomes more strongly confined. In the absence of bulk flow, escape is often estimated as the fraction of upward moving atoms/molecules at the nominal exobase with velocities exceeding the escape velocity, v_{esc} . This gives the Jeans flux: $\phi = [n_{\text{exo}} \langle v \rangle / 4] [1 + \lambda] \exp(-\lambda)$, where n_{exo} is the density at the exobase, $n(r_{\text{exo}})$, and $\langle v \rangle$ is the mean thermal speed ($\langle v \rangle = (8kT/m\pi)^{1/2}$). In the limit that $\lambda \rightarrow 0$ in the exobase region, the atmosphere is no longer bound and blows away with a flux $= (n_{\text{exo}} \langle v \rangle / 4)$ similar to the outflow from a comet. Bodies with values of $\lambda < \sim 50$ at the exobase have extended atmospheres with $r_{\text{exo}}/r_p > \sim 1.2$ (Strobel 2002) where r_p is the planetary/satellite radius. Pluto has $\lambda \sim 10$ at $r_{\text{exo}}/r_p \sim 3.5$ (Strobel 2008b), whereas Venus, Earth and Mars have $\lambda \sim (350, 130, 200)$ at $r_{\text{exo}}/r_p \sim 1.02, 1.08, 1.05$ and Titan is intermediate with $\lambda \sim 45$ at $r_{\text{exo}}/r_p \sim 1.6$.

Since the tail of the Maxwellian energy distribution is depleted by escape, the Jeans expression implies that this portion of the energy distribution is rapidly replenished. Recently, Cui et al. (2008) examined this assumption solving the collision dominated flow equation obtained in the so-called 13 moment approximation (Schunk 1975). This accounts for

the perturbation in the Maxwellian energy distribution in a region in which the thermal gradients are not small. For H_2 above Titan's exobase they suggested that the upward component of the tail of the distribution is enhanced by thermal collisions, enhancing the Jeans escape rate, although that has been questioned.

15.2.2 Hydrodynamic Escape

For the lower values of λ (~ 50), well above the blow-off condition, a controlled outward expansion of the atmosphere, called slow hydrodynamic escape, has been suggested to occur in planetary atmospheres. This process is assumed to be driven by solar EUV and UV heating and upward thermal conduction (McNutt 1989; Krasnopolsky 1999; Strobel 2008a; see Johnson et al. 2008 for a description). In this model of the thermosphere, the fluid equations *below* the exobase are solved under the assumptions that the escape flux, ϕ , is significant and hydrostatic equilibrium is a reasonable approximation (i.e., flow speed is much less than $\langle v \rangle$). The 1D radial continuity, momentum and energy equations are scaled by the escape flux, ϕ , as well by λ and T . The kinetic energy of the flow is dropped from the energy and momentum equations and an optimal solution, adjusting the escape flux, is sought starting from the lower boundary up to the exobase. The scaling of the equations by ϕ favors solutions with a significant escape flux. An upward flow is extracted from the 'best' solution to the scaled equations below the exobase by matching the model to the measured density profiles. Although the flux of molecules at the exobase with speeds above the escape speed is much too small to account for the extracted escape flux, the model is continued *above* the exobase where the energy is assumed to be supplied by upward thermal conduction (Strobel 2008a, 2009). That is, thermal conduction is assumed to collisionally enhance the tail of the thermal distribution adding to the escape flux (Yelle et al. 2008; Strobel 2008a). An upper limit to the mass escape flux is obtained by equating the gravitational energy per unit time that would be carried off by the escaping particles to the heating rate $\{[GMm/r_0] (4\pi\phi_{\max})\} \approx \int_{r_0}^{\infty} Q 4\pi r^2 dr$, where r_0 is the lower boundary and Q is the net solar heating/cooling rate, a quantity that varies with composition.

Due to the upward flux, adiabatic cooling occurs so that the temperature gradient is slightly negative in the thermosphere below the exobase. Above the heating maximum (or the lower boundary to the region described, whichever is highest), upward thermal conduction delivers the energy for the expansion. Since the fluid expression used for conduction begins to fail as Kn increases above about 0.1, and fails dramatically above the exobase, solutions below the

exobase should be matched to a kinetic model of the exobase region and corona (e.g., Marconi et al. 1996; Tucker and Johnson 2009). Later in the chapter the results of Monte Carlo simulations of the transition region are examined. These simulations indicate that thermal conduction can not produce the proposed escape fluxes for the values of λ that are relevant to Titan's exobase region.

15.2.3 Photochemical-Induced Escape

Photochemical-induced escape occurs in response to the solar UV and EUV absorbed by molecules in the thermosphere and corona. A fraction of the energy absorbed leads to dissociations and exothermic reactions that produce atoms and molecules with energies ($\sim eV$) that exceed the escape energy. If these events occur in the thermosphere near the exobase or in the corona above the exobase, and the products are moving radially outward, they can escape to space and contribute to atmospheric loss.

The photochemical-induced escape of N_2 , CH_4 , H , H_2 , N , NH , HCN , CN and small hydrocarbons at Titan has been recently studied (De La Haye et al. 2007b). The escape rates were calculated for 12 species, a subset of 19 species and 47 processes examined earlier (Cravens et al. 1997). To calculate the escape fluxes, they integrated the production profiles from the exobase to 2500 km above Titan's surface. Using the 2-stream approximation for hot atoms and molecules moving through a background mixture of N_2 , CH_4 , and H_2 , the photochemical escape rates for N and C in all forms were estimated to be relatively small, $\sim 1.3 \times 10^{26}$ amu/s and $\sim 0.86 \times 10^{26}$ amu/s respectively.

A much larger escape rate for nitrogen ($\sim 0.3 \times 10^{28}$ amu/s; D. Shemansky private communication) was recently estimated based on UVIS measurements (e.g., Gustin et al. 2009). Solar occultation measurements of UV emissions during T10 and T26 produced line of sight column densities vs distance from the surface. These nitrogen emissions were interpreted as caused by photo-dissociative excitations leading to the production of hot recoils, a fraction of which have escape energies. Photodissociation of nitrogen was also the dominant heat source at ~ 1300 km in the model of Strobel (2008a)

15.2.4 Plasma-Induced Escape

For an unmagnetized body like Titan, the magnetospheric plasma and fields can interact with the corona and the exobase region of the thermosphere which can induce escape by a number of processes. However, the role of the plasma and fields in causing mass loss from Titan can vary considerably

depending on whether Titan is in or out of Saturn's magnetospheric current sheet, where ion pressures are high ($\beta \gg 1$) and composition is dominated by heavy ions, or Titan is at higher magnetic latitudes where composition is dominated by light ions, densities and plasma pressures are low ($\beta \ll 1$) (Chapter 16) or Titan is outside the magnetosphere where solar processes dominate. Here β is the ratio of the plasma pressure to the magnetic pressure: $\beta = n_i kT_i / (B^2 / 2\mu_0)$ where n_i and T_i are the density and temperature of the ions, B the magnetic field and μ_0 is the permeability of space. This variation in upstream conditions can be traced to Saturn's magnetosphere being in a magnetodisk configuration at Titan's orbital position for local times away from noon where the field is more dipolar (Bertucci et al. 2008; Chapter 16). The current sheet regions are referred to as high energy input cases and the lobe like field regions are referred to as low input energy cases in Chapter 16. For the high energy case, Titan's induced magnetosphere will be more compressed and the ion gyroradii will be greater than Titan's radius, so that the energy input to Titan's ionosphere will be higher and heavy pick-up ion losses will be greater. In the low energy limit, Titan's induced magnetosphere will be less compressed and the ion gyroradii smaller since light ions dominate, so that the ion energy input to atmosphere will be lower. Magneto-hydrodynamic (MHD) and hybrid models of the interaction have been used for describing *both* the high and low energy limits. In the high energy limit, a hybrid simulation is often favored in order to account for the ion gyromotion and drifts. Since the low energy limit is more fluid like, MHD models are often favored. Another limiting case occurs when Titan is outside the magnetosphere and exposed to either the magnetosheath or the solar wind (Penz et al. 2005). In the case of the solar wind or magnetosheath, the composition is dominated by light ions but the pickup energies can be much higher due to the greater upstream speeds ~ 400 km/s (Sittler et al. 2006). Other effects also produce a highly variable ambient plasma pressure (e.g., Ma et al. 2006; Sillanpaa et al 2006).

The morphology of the induced fields and the radial scale of the exobase compared to the ion gyroradius determine the nature of magnetosphere/atmosphere interaction (e.g., Chapter 16) and the rate of atmospheric loss. Ionization in the exosphere and upper atmosphere can lead to loss by the outflow of ions from Titan's ionosphere, as is the case at Venus (e.g., Ma et al. 2008). In addition, pick-up ion formation can lead to loss if the freshly produced ions are swept down the tail of the interaction region (Chapter 16; Hartle et al. 1982; Wahlund et al. 2005; Coates et al. 2007). Such ions flowing through the corona can efficiently heat the atmosphere in the exobase region due the long-range ion-neutral interactions. Following ionization by charge exchange, energetic neutral atoms (ENAs) are formed which can escape Titan's gravity (Mitchell et al. 2005; Garnier et al. 2007, 2008; Smith et al. 2009).

A fraction of the pick-up ions and ENAs can re-impact the atmosphere with enough energy to induce heating and atmospheric sputtering (Michael et al. 2005a; Michael and Johnson 2005). This is particularly true when the pick-up ion gyroradius is of the order of the planet radius as is the case when heavy ions dominate, the high energy limit discussed above. Below we convert the loss estimates to global averages, even though there are considerable asymmetries in the plasma flux and the escape flux: e.g., pick-up ion impacts primarily occur on the Saturn side of Titan's trailing hemisphere (e.g., Hartle et al. 1982) whereas the location of the dominant photo-ionization rate changes as Titan orbits (e.g., Fig.15.1b).

The sputtering efficiency produced by the incident plasma is often given as a yield. It is the ratio of the number of escaping particles to the number of incident particles and varies inversely with the escape energy at the exobase (e.g., Johnson 1990). Sputtering of an atmosphere can occur by direct scattering of atmospheric molecules, also called knock-on, which dominates at grazing incidence. For heavy incident ions which can puncture the magnetic barrier of Titan's induced magnetosphere and penetrate the exobase, a cascade of recoils is set in motion with some having sufficient energies and the appropriate direction of motion to escape (e.g., Johnson 1994). This occurs at Titan due to the incident ambient plasma ions, such as O^+ , the pickup ions, such as N_2^+ and CH_x^+ , and the heavy ENAs. These cause both heating of the thermosphere near the exobase and escape as shown in simulations prior to Cassini's arrival at Titan (Shematovich et al. 2003; Michael et al. 2005a; Michael and Johnson 2005).

15.3 Simulations of the Transition Region and Escape

In the transition region the Maxwellian energy distribution can develop a non-thermal tail due the breakdown of thermal equilibrium and, more dramatically, due to the local production of hot recoils by the solar UV or the incident plasma (e.g., Fig. 15.2). In the exobase approximation described above, the fully collisional fluid approximation is used below the exobase and a ballistic, collisionless model is used above the exobase. Analytic expressions for the density vs altitude can be obtained by direct integration of the trajectories (Johnson 1990; appendix) or using the Louisville theorem (e.g., Schunk and Nagy 2000). However, the evolution of the initially energized atoms and molecules and their recoils can be described *throughout the transition region* using the Boltzmann transport equation for each molecular species or by Monte Carlo simulations.

15.3.1 Boltzmann Equation

Because solving the full set of transport equations is difficult, various approximations are used. The two stream model (Nagy et al. 1981) has been used on a number of planetary atmospheres and for analyzing the photochemistry in Titan's upper atmosphere normalized to Cassini ion-neutral mass spectrometer (INMS) data (DeLaHaye et al. 2007b). In addition, INMS H₂ data were analyzed using the collision dominated 13-moment equation, essentially the Navier–Stokes equation (Hirschfelder et al. 1964; Schunk 1975; Schunk and Nagy 2000), to describe the perturbations to the behavior of the atmosphere in a transition region (Cui et al. 2008).

A useful analytical approximation for the energy spectrum of the hot recoils has also been derived from the Boltzmann equation by ignoring spatial and temporal variations in the atmosphere (Johnson 1990, 1994). In a single component atmosphere, the number of hot recoils with energy between E and $E + dE$ produced by a primary particle of energy E_0 is given by: $\eta(E_0, E)dE \approx \beta(E_0/E^{2+x})dE$ (Johnson 1990, 1994). This applies for $E \gg kT$, where T is the atmospheric temperature, and β and x vary slowly according to the form for the interaction potential between a hot recoil and an atmospheric molecule. For a steeply varying potential, $\beta \approx 6/\pi^2$ and $x \approx 0$ has been shown to be consistent with data (Sigmund 1981; Johnson et al. 1994). In steady-state, the number of moving atoms with energy between E and $E + dE$ produced by a source rate $\phi(t)$ of hot particles of energy E_0 can be written $[\phi(t)/v(E)][\delta(E_0 - E) + \eta(E_0, E)]dE$. Here the delta function, $\delta(E_0 - E)$, accounts for the initial recoil and $v(E)$ is the collision frequency between a hot molecule and a thermal molecule: $v(E) = [vn\sigma_d(E)]$, where v is the relative collision velocity: e.g., $v = (2E/m)^{1/2}$ with m the mass of the atmospheric recoil (Johnson 1994) and σ_d is the diffusion cross section. Monte Carlo simulations using realistic potentials have been carried out confirming this analytic model (e.g., Johnson et al. 2000; Johnson 2009). These expressions apply to the recoil production and collisional cooling of the hot atoms and molecules produced by either photo-chemistry or the incident plasma (Johnson 1994; Johnson et al. 2000). Such a model was used to fit Titan's observed coronal densities (DeLaHaye et al. 2007a).

15.3.2 Monte Carlo Simulations

Direct Simulation Monte Carlo (DSMC) calculations have also been used to describe the fate of hot recoils and escape (e.g., Michael and Johnson 2005). This is a stochastic method used to simulate a rarefied gas and is equivalent to solving the Boltzmann equation. It treats both the dynamic

and stochastic nature of the gas (Bird 1994). Each species is described in terms of its phase space distribution with changes in the distributions determined by collisions between atmospheric particles (e.g., Marconi et al. 1996). Collisions with incident ions can also be included (e.g., Michael et al. 2005a; Krestyanikova and Shematovich 2006). The motions of representative particles, each assigned a weight, are calculated taking into account collisions and external forces (e.g., gravitational fields for neutrals and electro-magnetic fields for ions). DSMC is time consuming when the domain is highly collisional, but is useful for describing the transition from the collisional to collisionless regime (e.g., Marconi et al. 1996; Leblanc and Johnson 2001; Michael and Johnson 2005).

Because large numbers of particles are needed to obtain an accurate speed distribution over the transition region, approximations are often used. In exosphere approximation described above, Monte Carlo models of the phase space distributions have been used to describe the ballistic, collisionless corona. A significant improvement is referred to as the test particle method. The velocity space is divided into a hot particle population (the tail of the distribution) and a thermal background. The hot component or trace species are then tracked throughout the transition region and into the corona. These atoms and molecules move in the background atmosphere allowing collisions only with the thermal background atmosphere (e.g., Shematovich et al. 2003). This is equivalent to solving a linearized Boltzmann equation. 1D test particle simulations were compared to full DSMC simulations and the analytic model described above using a realistic interaction potential (Johnson et al. 2000). They showed that if the escape energy is well above the thermal energy, the escape rates obtained using test particle simulations compared favourably with DSMC results using realistic potentials. Both methods differed from simulations using hard sphere collisions. However, in the full DSMC model the energy spectra in the exobase region differed significantly from a Maxwellian with a power law tail, more closely resembling a kappa distribution (Johnson et al. 2000). Leblanc et al. (2002) described the effect on atmospheric sputtering when the exobase is dominated by molecules rather than by atoms.

Monte Carlo simulations have rapidly increased in complexity and are more useful than solving the Boltzmann equations when there are multiple species. The simpler test particle methods are sufficient for escape unless the response of the atmosphere is significant. In addition, test particle methods below the exobase can be coupled to DSMC models in the exobase region and above. However, in order to describe the evolution of the velocity distribution from the thermosphere across the exobase into the corona, and the proposed ability of thermal conduction to drive escape, DSMC simulations are required which span the full exobase region: $Kn > \sim 0.1$ (e.g., Marconi et al. 1996).

15.4 Estimates of Escape Flux: Pre-Cassini

Mass loss from Titan's thick and extended atmosphere induced by the ambient plasma ions, pick-up ions, ionospheric outflow and energetic re-impacting neutrals have been calculated by a number of groups. Initial estimates of the photon and electron-induced chemistry near the exobase gave very large loss rates (Strobel and Shemansky 1982), but revisions resulted in more modest rates, $\sim 2 \times 10^{26}$ amu/s (Shematovich et al. 2003). Initial estimates for atmospheric sputtering induced by magnetospheric ions penetrating Titan's atmosphere were also very large (Lammer and Bauer 1993). However, a direct simulation Monte Carlo (DSMC) model of the sputtering and heating using a model plasma flux consisting of magnetospheric and pick-up ions led to a few degrees increase in the exobase temperature (Michael and Johnson 2005) and a globally averaged loss rate: $\sim 5 \times 10^{26}$ amu/s (Michael et al. 2005a). Therefore, prior to the arrival of Cassini-Huygens, it was concluded that the present escape rate for carbon and nitrogen species was $\sim 5 \times 10^{26}$ amu/s and dominated by atmospheric sputtering (e.g., Shematovich et al. 2003). If this is the case, then the observed nitrogen isotope ratios must have evolved in an earlier period when the solar EUV and plasma interactions were more robust (e.g., Lammer et al. 2008; Chapter 7) or never evolved at all (Mandt et al. 2009).

Following Voyager it was also assumed that nitrogen escaping from Titan would be the dominant process for supplying Saturn's magnetosphere with heavy ions (Barbosa 1987). However, ions formed near Titan's orbit from the ejected neutrals have a high probability of being lost down Saturn's magnetotail or being lost from this region by an injection event. Therefore, the dominant source of nitrogen ions to Saturn's magnetosphere has been shown to be Enceladus (Smith et al. 2007, 2008). After reviewing the recent estimates of the escape rate, we also compare the various sources of neutral and ions for Saturn's magnetosphere.

15.5 Estimates of the Escape Flux: Cassini Data

With the many transits of Titan's exobase by Cassini, the escape processes have been re-examined. Modeling based on the Cassini data set appear to suggest larger heavy molecule loss rates than the most recent preCassini estimates. However, this modeling also indicates that the dominant heating processes for Titan's atmospheric corona and exobase region are not fully understood and can vary considerably with solar illumination angle and plasma pressure. Table 15.1 gives the principal estimates of mass loss both pre-and post

Table 15.1 Escape rates

Atmospheric component	Escape process	Loss rate
(in 10^{28} amu/s ≈ 0.2 Titan Atmospheric Masses/4 Gyr)		
Pre Cassini		
H ₂ ^a	Jean's escape	~1–3
CH ₄ ^b	Destruction/precipitation	~10–30
C, N ^c	Photochemistry and sputtering	~0.01–0.06
Based on Cassini Data		
Ions ^d	Pickup/outflow	~0.01–0.05
H ₂ ^e	Thermal escape	~0.8–2
CH ₄ ^f	Destruction/precipitation	~24
N ₂ /CH ₄ ^g	Corona fits (<~2000 km)	~0.00–0.16
N ₂ /CH ₄ ^h	Sputtering	~0.3–3.6
CH ₄ ⁱ	Hydrodynamic	~4–5
CH ₄ + H ₂ ^j	Hydrodynamic	~4.5

^a(e.g., Lebonnois et al. 2003)

^b(Wilson and Atreya 2004)

^c(Michael et al. 2005a; Shematovich et al. 2003; Cravens et al. 1997; Lammer and Bauer 1993; Strobel et al. 1992; Gan et al. 1992; etc.)

^d(Hartle et al. 2008; Wei et al. 2007; Coates et al. 2007; Ma et al. 2006; Sillanpaa et al. 2006; Wahlund et al. 2005; etc.)

^e(Cui et al. 2008; Garnier et al. 2008; Bell et al. 2009)

^f(based on the H₂ data in Cui et al. 2008 and model of Wilson and Atreya 2004; Mandt et al. 2009)

^g(DeLaHaye et al. 2007a based on kappa fits)

^h(DeLaHaye et al. 2007a; average for 5 passes based on analytic model and coronal structure)

ⁱ(Yelle et al. 2008)

^j(Strobel 2008a, 2009)

Cassini. Rates are given in units of 10^{28} amu/s, which is ~ 0.2 of the present Titan atmospheric mass lost in 4 Gyr.

15.5.1 H₂ Escape

Data from the Cassini ion-neutral mass spectrometer (INMS) indicate a steeply varying H₂ density profile above the nominal exobase (Waite et al. 2005) as seen in Fig. 15.3a. This profile is consistent with diffusion of H₂ through the Titan atmosphere resulting in a large escape rate: a mass flux of H₂ $\sim 1 \times 10^{10}$ amu/cm²/s normalized to the surface of Titan (Cui et al. 2008; Bell et al. 2009). Assuming this rate is global ($\sim 1.6 \times 10^{28}$ amu/s), then it is comparable to the pre-Cassini estimates. A large H₂ escape flux is consistent with the presence of the extended hydrogen corona imaged by the detection of energetic neutral atoms produced by charge exchange with protons (Garnier et al. 2007, 2008).

In their analysis Cui et al. 2008 extracted an exobase temperature for hydrogen that was slightly lower than that for the principal species. They interpreted the cause to be the significant escape rate. When they used their lower H₂ temperature, they estimated that the loss rate was larger than

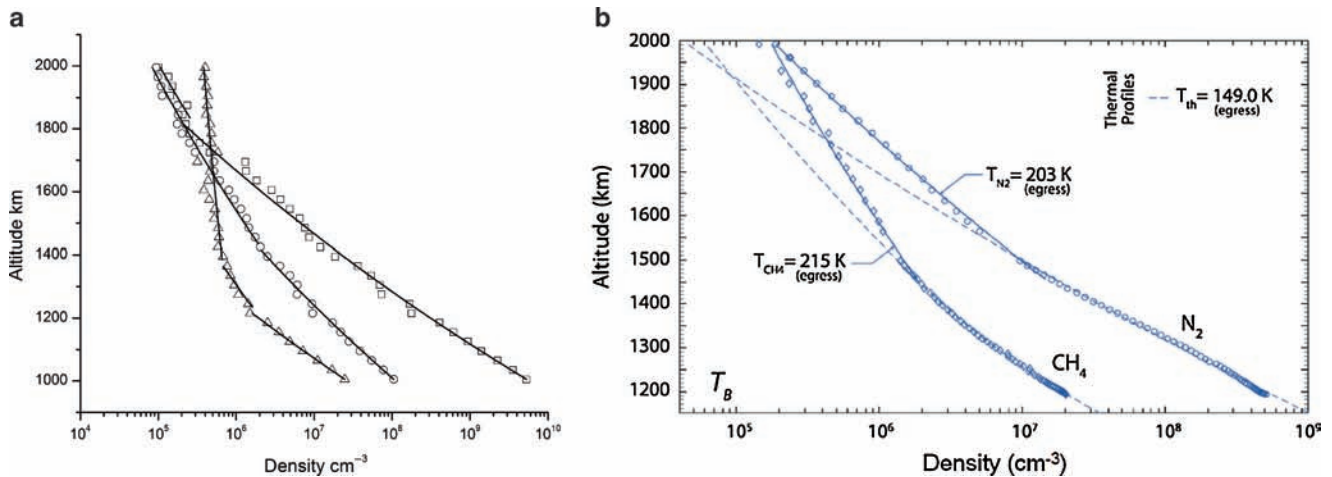


Fig. 15.3 (a) Density profiles for H_2 (triangles), CH_4 (circles) and N_2 (squares) based on an average of INMS ingress and egress data during 18 passes through Titan's exobase (data from Magee et al. 2009); (b) density vs radial distance from Titan for CH_4 and N_2 from the INMS data for Tb egress (from Fig. 6 in DeLaHaye et al. 2007a):

dashed lines are the assumed isothermal fits based on data below the exobase (~ 1450 km); this shows a change in slope of the density profiles above the nominal exobase. The exobase temperatures and especially the slope of the profile above the exobase are highly variable.

that for the Jeans escape. Based on a collision-dominated flow equation, they concluded that Jeans escape was enhanced. They proposed this was due to thermal conduction in the exobase region causing a distortion in the Maxwell Boltzmann energy distribution. Bell et al (2009) find the hydrogen loss rate is consistent with Jeans escape.

15.5.2 Carbon Mass Loss by Precipitation

Since hydrogen is produced by dissociation of methane and other hydrocarbons, its loss to space implies that atmospheric methane is also lost to the surface in the form of precipitating hydrocarbon molecules and small carbonaceous grains that form in the atmosphere following dissociation of methane. Based on the H_2 escape rate and the chemistry model of Wilson and Atreya (2004), methane is lost by precipitation at a rate $\sim 2 \times 10^{29}$ amu/s (e.g., Chapter 8; Mandt et al. 2009). Therefore, even for the largest escape rates for methane and nitrogen discussed below, *atmospheric mass loss to the surface dominates mass loss by escape*.

Because the cross section for photo-absorption by methane in the UV-EUV is relatively large, the loss of methane by dissociation, reaction and precipitation affects the modeling of diffusion in Titan's upper atmosphere. That is, ignoring other effects, an upward diffusive flux is required to replace the destroyed methane: the mass flux is $\sim (m_{CH_4} / \sigma_{abs} \tau_{CH_4}) [1 - \exp(-\sigma_{abs} N_{CH_4})]$, where m_{CH_4} is the mass of methane, τ_{CH_4} is the lifetime of CH_4 exposed to the solar flux and the magnetospheric electrons above the exobase, and σ_{abs} is the average attenuation cross section of the radiation. The downward carbon flux decreases with

increasing altitude (Sittler et al. 2009; Mandt et al. 2009) and the prefactor, $(m_{CH_4} / \sigma_{abs} \tau_{CH_4})$, is equal to the integrated methane loss rate by this process *above* the peak in the methane destruction rate. That is, assuming the destruction of methane occurs over the disc, then one fourth of the exobase area times the pre-factor must roughly equal the integrated precipitation rate, $\sim 2 \times 10^{29}$ amu/s. Methane can also be destroyed by reaction with nitrogen atoms and ions, which can dominate at high altitudes (Mandt et al. 2009). The upward diffusive flux required to replace the methane lost by this process must be included in any model of the INMS density profiles (Chapter 8).

15.5.3 Escape of Nitrogen and Carbon: Hot Recoil Models

Based on UVIS observations (e.g., Gustin et al. 2009) the loss rate of N atoms was estimated to be $\sim 2.0 \times 10^{26}$ N/s ($\sim 0.3 \times 10^{28}$ amu/s) (D. Shemansky, private communication). This is much larger than the photo-chemical loss rate of nitrogen in DeLaHaye et al. (2007b) ($\sim 1.3 \times 10^{26}$ amu/s). However, it is close to the favored loss rate estimated in DeLaHaye et al. (2007a) in order to explain Titan's coronal density structure as discussed below.

INMS data for a number of early passes were examined (DeLaHaye et al. 2007a) assuming that the atmospheric structure near the exobase could be understood if the energy spectra of the molecules in the corona had a significant non-thermal, 'hot', component. That the production of hot recoils might be occurring is indicated by the UVIS results for nitrogen but was earlier suggested by the change in slope of the density vs altitude near the nominal exobase. This is seen in

Fig. 15.3b as Cassini crossed the exobase region while exiting Titan's atmosphere on orbit Tb. A change in the slope is even suggested, though more subtly, in Fig. 15.3a by the N_2 density profile vs altitude averaged over many passes through Titan's atmosphere. In addition it is clear from the five passes through the exobase examined by DeLaHaye et al (2007a), that the coronal structure varies significantly both in space and in time. This variability has been confirmed by the analysis of many additional orbits (Bell et al. 2009).

In order to simulate the densities of N_2 and CH_4 above the nominal exobase, ~ 1450 km, up to 2000 km above Titan's surface, expressions obtained from the Louisville theorem were used (DeLaHaye et al. 2007a). This is equivalent to a Monte Carlo ballistic trajectory model of the corona (Johnson 1990). Molecules are launched from the exobase with a chosen energy spectrum and the density vs altitude is calculated. A number of forms for the energy spectra were used and tested against Cassini data for the CH_4 and N_2 coronal structure. As shown in Fig. 15.4, results were presented for two models of the molecule energy spectrum: a thermal spectrum with a tail given by the analytic model described above and an energy spectrum described by a kappa function. They found that over the range for which they had data, the distribution of molecules in the hot corona could be better represented by a kappa distribution (Vasyliunas 1968; Jurac et al. 2002). These energy distributions are Maxwellian at the lower energies but decay as power laws at the higher energies. Such a distribution at the exobase implies that an equilibrium thermal energy distribution well below the exobase develops an enhanced tail in the exobase region. The enhanced tail was assumed to be produced by energy deposition in the transition region which they hypothesized was a result of the interaction with the local plasma. Such a smoothly varying distribution, rather than a Maxwellian with a power law tail, is also consistent with DSMC simulations of energy deposition into an atmosphere in the form of hot recoils (Johnson et al. 2000).

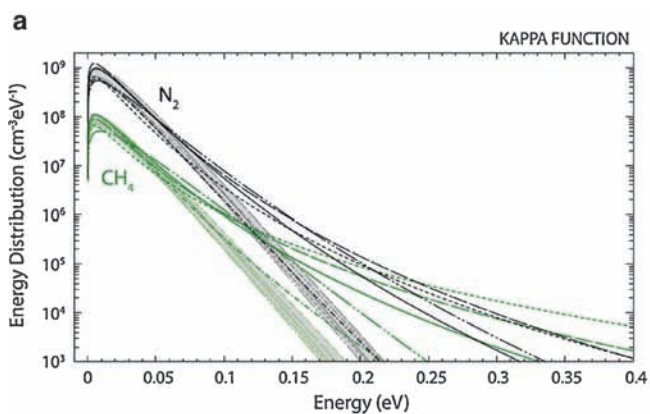
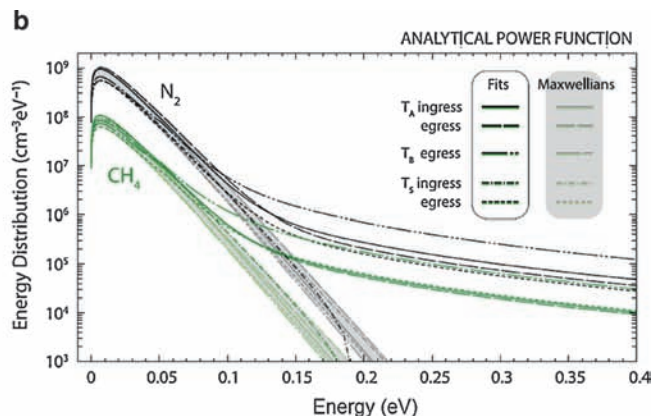


Fig. 15.4 Energy spectra at the exobase for five crossings of the exobase showing the Maxwellian (shaded profiles) and the tail of the distribution containing the hot recoils: (a) energy spectra are described by a kappa function and resulting densities are fit to the INMS density data in the

DeLaHaye et al. (2007a) found that for those Cassini passes through Titan's atmosphere for which a hot nitrogen corona was detected, the extracted kappa distributions exhibited tails that decayed much more steeply than the analytic recoil spectra discussed above: powers ~ 4 – 20 . This steep decay (e.g., Fig. 15.4a) could be an artifact of the narrow range of modeled altitudes or could suggest that processes other than the production of hot recoils are responsible for the coronal structure. Although kappa fits up to only 2000 km can not give a good measure of the escape flux, they can give a measure of the amount of energy needed to form the observed hot corona. However, for four of the five exobase crossings examined, they *could not* account for the measured corona structure by assuming that the tail of the distribution was only populated by photon- and electron-induced chemical processes or by the published models of the plasma-induced heating rate. Although Yelle et al. (2008) and Strobel (2009) suggested the effect of the plasma flux is small, additional heating in the exobase region appears to be required. This must occur by energy transport from below, by horizontal transport of energy, or by larger photo- and/or plasma energy deposition rates than initially assumed.

The estimates of the required heating rate in Table 15.2 were extracted from fits to the neutral densities using both models of energy spectra at the exobase. This energy could be deposited by exothermic chemistry, by interaction with the plasma, or by vertical or horizontal heat transport. The heating rate required was found to vary considerably from a crossing of the exobase in which no hot corona was identified, hence, no hot particle production in the exobase region was required, to relatively large energy deposition rates. For the five crossings examined *average* heating rates were obtained using the kappa and the analytic model for the recoil spectrum: ~ 95 eV/cm³/s and ~ 200 eV/cm³/s respectively (Table 15.2). Similar results were found for the analysis of a much larger set of orbits using kappa functions (J.



corona; (b) same but with the analytic model due to hot recoils added to the Maxwellian (from DeLaHaye et al. (2007a)). Escape energies at nominal exobase (1450 km): $CH_4 \sim 0.38$ eV; $N_2 \sim 0.67$ eV. Highest altitude was 2000 km corresponding to $\sim 12\%$ of the escape energy.

Westlake private communication). The extracted energy deposition rates are larger than the estimated photo-induced heating plus cooling rate at that altitude (~ 8 eV/cm³/s; Strobel 2008a) and the pre-Cassini estimates of the globally averaged plasma-induced heating rate (~ 15 eV/cm³/s, Lammer et al. 1998; ~ 25 eV/cm³/s, Michael and Johnson 2005), but are closer to the rates obtained by assuming the incident plasma flux is dominated by low energy ions as seen in Fig. 15.5.

Table 15.2 Energy deposition and Escape rates (DeLaHaye et al. 2007a)

Titan pass	T_{exo} (K) ^a	Energy deposition (eV/cm ³ /s) ^b	Escape flux (10 ⁹ amu/cm ² /s) ^c
TA ingress	150	82 [190]	0.02 [<18] (0.8–1.9)
TA egress	157	73 [150]	0.21 [<14] (0.7–1.5)
TB egress	149	250 [510]	0.00 [<48] (2.5–5.1)
T5 ingress	162	0 [0]	0.00 [<0.0] (0.0)
T5 egress	154	70 [130]	0.82 [<12] (0.7–1.3)
Average Global ^d (10 ²⁸ amu/s)			0.04 [<4] (0.2–0.4)

^aExobase temperature extracted from INMS density vs altitude below the exobase.

^bEnergy densities extracted from best kappa fits to speed distributions describing the corona density vs altitude from 1450 to 2000 km: Sum of energy deposition in N₂ and CH₄ from Table 6; [] same using the analytic model for the recoil spectrum discussed earlier with $x \sim 0$ (Johnson 1994); data from Table 5.

^cFlux at nominal exobase (1450 km): values from tail of kappa function fit to corona density from Table 6; [] analytic recoil model fit to coronal densities were described as upper limits from Table 5; () based on the energy deposition rates from the kappa and analytic model fits in column 2 scaled to recoil production and sputtering results in Michael et al (2005a): loss rate at exobase $\sim 25 \times 10^7$ amu/cm²/s for energy deposition rate ~ 25 eV/cm³/s, or a factor of $\sim 10^7$ amu (cm/eV); for normalization of fluxes to the physical surface multiply by 2.4: i.e. exobase area 2.04×10^{18} cm² vs surface area 0.84×10^{18} cm².

^dAverage of fluxes from column 3 assumed global.

Based on this analysis DeLaHaye et al (2007a) assumed that the plasma-induced heating associated with the magnetosphere–ionosphere interaction was more robust than pre-Cassini estimates. This might be consistent with the Cassini plasma science instrument (CAPS) observation of a low energy ion flux in the corona near the exobase (e.g., Fig. 15.6). Such ions transfer energy more efficiently to the neutrals and therefore deposit a large fraction at higher altitudes as seen in Fig. 15.5. These energies were *absent* from the early hybrid

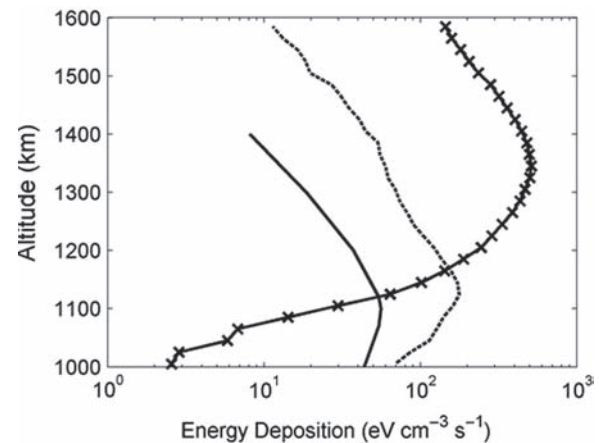
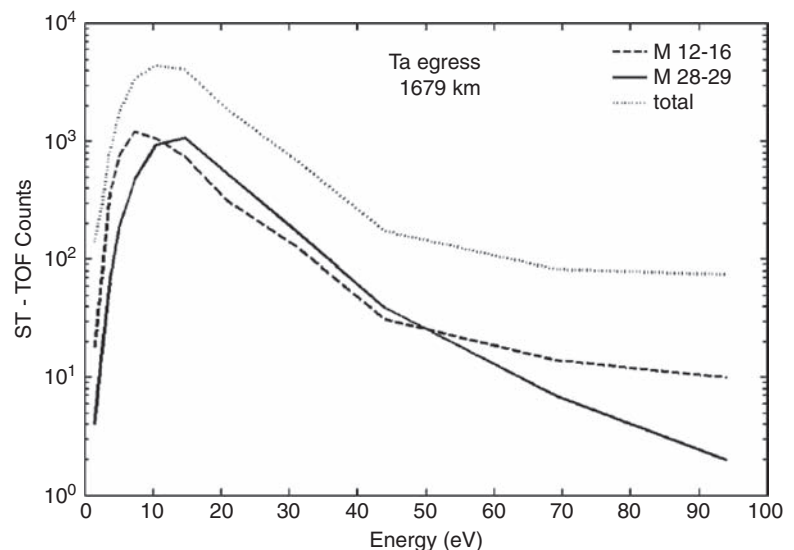


Fig. 15.5 Comparison of energy deposition rates in eV/cm³/s vs radial distance from Titan's surface: (*solid line*) the globally averaged solar EUV/UV at medium solar conditions: net heating with 25% efficiency and HCN cooling ($\sim 12\%$ of total near exobase) (Strobel 2008a); (*dashed line*) the model of the incident plasma used in Michael and Johnson (2005) based on a globally averaged flux of $\sim 5 \times 10^9$ eV/cm²/s at the exobase. This only includes that component of the energy going into the *production of recoils*; it also accounts for losses due to escape and to the vibrational, rotational and dissociation processes. Cooling due to emissions is not included. (*Solid line with crosses*): the same energy flux as dashed curve but the energy spectra in Fig. 15.6. This results in higher energy deposition rates near the exobase. Although the energy flux was the same the escape rate of recoils increased roughly proportional to the energy deposition rate as shown by model calculations and assumed in creating Table 15.2 (DeLaHaye et al. 2007a).

Fig. 15.6 Energy distribution for ions above Titan's exobase (~ 1680 km) on the ingress portion of Cassini orbit Ta obtained from CAPS ST-TOF data: results are given for the two principal heavy ions mass peaks 12–16 and 28–29 amu, as well as a total (Michael et al. 2005b). Model plasma ion energy spectra used in simulations of atmospheric sputtering (e.g., Shematovich et al. 2003) and in obtaining the dashed curve in Fig. 15.5a had a lower cut-off at ~ 50 eV.



simulation that was used to obtain the pre-Cassini plasma heating rate. Such energies are associated with pick-up of ions close to the exobase and/or ionospheric out flow (ions driven out of the ionosphere by the plasma pressure and scavenged by pick-up) (Wahlund et al. 2005; Ma et al. 2006; Sillanpaa et al. 2006; Hartle et al. 2006b; Chapter 16). For this reason the simulations in Michael et al. (2005a) were repeated using the same net heavy ion energy flux onto the exobase, but with an ion energy spectrum consistent with that in Fig. 15.6. Not surprisingly the energy deposition rate near the exobase increased dramatically. Although such a high rate is unlikely, the increase in the mass loss rate by sputtering is found to roughly scale with the energy deposition rate near the exobase.

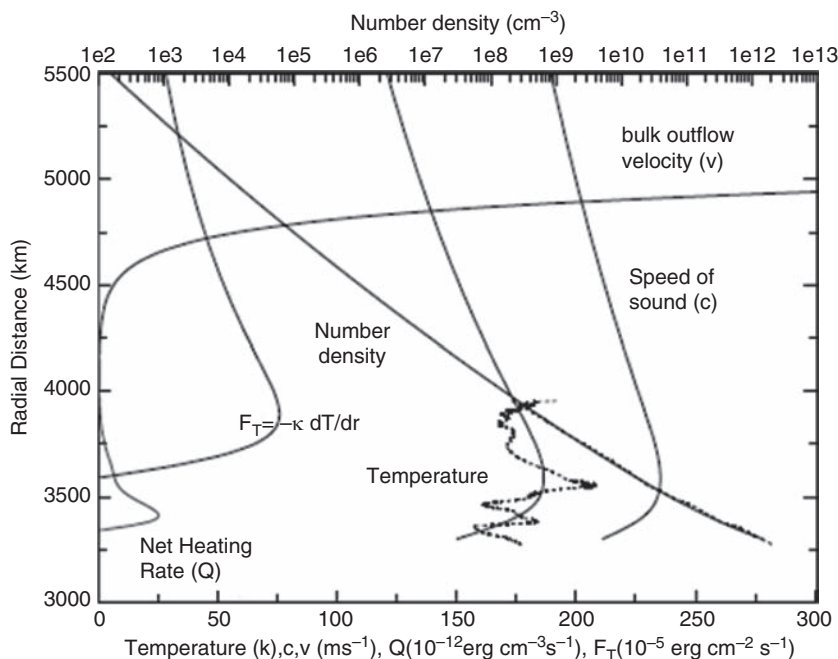
The kappa energy spectra extracted from the fits to the INMS data (Fig. 15.4a) are seen to have high energy tails that decay more steeply than does the analytic model of the recoil distribution (Fig. 15.4b). Since escape rates are determined by the tail of the distribution they are very different in the two models as seen in Table 15.2. However, the tails of the distribution are not accurately tested by the atmospheric density data below 2000 km. The kappa distributions rates are heavily dominated by loss of CH_4 , whereas those for the analytic model are not. It is seen that the heating rates extracted in the two models are much closer in size. Therefore, assuming the heating rates are due to a production of recoils, atmospheric loss rates were better estimated by scaling to the Monte Carlo model in Michael et al. (2005a). As demonstrated by the two simulations in Fig. 15.5, this scaling is valid as long as the primary recoils have energies much larger than the escape energy at the exobase (~ 0.38 eV for CH_4). Based on energy deposition rates extracted from the energy spectra in Fig. 15.4 (e.g., see Table 15.2) and scaling to the Monte Carlo simulations,

mass loss rates obtained for the two models of the energy spectrum are within a factor of two of each other (Table 15.2): $\sim 0.3 \times 10^{28}$ amu/s and with nitrogen loss somewhat larger than that of methane. This rate is much larger than the pre-Cassini estimates. A rough *upper bound* was also obtained using the analytic model of the hot molecule spectrum. Summing the CH_4 and N_2 contributions and averaging over the five passes gives an upper bound of global mass loss rate via the heavy molecules: $< \sim 4 \times 10^{28}$ amu/s. Therefore, globally averaged mass loss rates $\sim 0.3\text{--}4 \times 10^{28}$ amu/s are possible based on the analysis in DeLaHaye et al. (2007a).

15.5.4 Escape of Nitrogen and Carbon: Continuum Models

Describing Cassini data below the exobase using continuum models, Yelle et al. (2008) and Strobel (2008a, 2009) separately concluded that, in addition to H_2 loss, there is a significant escape flux of heavier molecules. These models did not include methane destruction in the thermosphere and estimated that the plasma heating rate was not important. Strobel used the slow hydrodynamic escape model described earlier to fit the HASI density and temperature profile. Three cases were examined: a lower boundary that allowed a heat flux, but no heating in the region modeled, and two different net heating/cooling rates with peaks occurring well below the exobase (e.g., Figs. 15.5 and 15.7). He concluded that the observed altitude dependence of the mass density and temperature (Fulchignoni et al. 2005) could be represented by having an upward mass flux $\sim 5 \times 10^{10}$

Fig. 15.7 A model for Titan's atmosphere (Strobel 2008a): n , T , c , v , and upward thermal heat conduction flux (solid lines) for an N_2 atmosphere with solar medium conditions: net heating due mostly to CH_4 UV heating above the lower boundary at $r_0 = 3300$ km, $T_0 = 158$ K, and downward thermal heat conduction flux at lower boundary = 4.0×10^{-3} erg/cm²/s. Comparison with the HASI measurements of total number density and temperature (dashed lines) at $\sim 10.3^\circ\text{S}$ latitude. Assuming the model applies above the nominal exobase (here ~ 4300 km), the solution is valid only to ~ 4750 km and the mass escape rate is 4.5×10^{28} amu/s. Solar heating near the exobase contributes only $\sim 10^{-3}$ of the heat conduction flux and plasma-induced heating is ignored.



amu/cm²/s with respect to Titan's surface (e.g., Fig. 15.7). Presuming this upward flux implied escape to space, the model was extended into the region above the nominal exobase with thermal conduction driving escape. Due to diffusive separation, the escape flux was estimated to be dominated by the lighter species, $\sim 2/3$ CH₄ and $1/3$ H₂ by mass for a total $\sim 5.6 \times 10^{28}$ amu/s (Strobel 2009). However, since the expression for heat conduction was not modified above the exobase where the mean free path between collisions is large, such results are questionable.

Yelle et al. (2008) analyzed the INMS ingress data averaged over many passes for the density vs altitude of CH₄ and N₂. The changing atmospheric composition with altitude in the thermosphere (e.g., Fig. 15.3a and b) was shown to be indicative of diffusion of CH₄ through the background N₂. In order to separate eddy and molecular diffusivity, they derived an eddy diffusion coefficient from the density profile for ⁴⁰Ar. They then solved the coupled diffusion equations using both eddy and molecular diffusion allowing for the possibility of upward flow. Modeling the averaged profiles up to nominal exobase, they found that the CH₄ and N₂ density profiles could be described if CH₄ flows upward at a rate of $\sim 4\text{--}5 \times 10^{10}$ amu/cm²/s consistent with the model at mid latitudes of Muller-Wodarg et al. (2008). They also presumed this upward flux was a measure of the escape flux and pointed out that the mass flux is close to that found by Strobel (2008a). It is also close to the average upper limit for escape in DeLaHaye et al. (2007a). Recently, Bell et al. (2009) show the INMS data can be explained by a larger range of methane escape rates. Therefore, all models of the Cassini data could *in principal* be consistent (Johnson 2009).

Although the density profile below the exobase can be reasonably well described by an isothermal atmosphere, modulated by gravity waves (Waite et al. 2005; Muller-Wodarg et al. 2006; Fulchignoni et al. 2005), the continuum models yielded temperature profiles in which T decreased with increasing altitude in the exobase region consistent with upward heat flow. A 2D model of the northern hemisphere, the region primarily sampled by Cassini (Muller-Wodarg et al. 2008), also shows decreasing T profiles, primarily at latitudes below $\sim 70^\circ$. Above that latitude the profiles are complicated resulting in significant temperature uncertainties.

15.5.5 Summary of Mass Loss: Cassini Data

Based on the UVIS measurements (D. Shemansky private communication) and the different models of the INMS and HASI data, Cassini data suggest that Titan could be experiencing an average mass loss rate to space of heavy molecules $\sim 0.3\text{--}5 \times 10^{10}$ amu/cm²/s. This large range of values is due to differences in the analysis of the data and is *not* related to the expected variability discussed earlier. Although all of these

papers suggest the heavy molecule loss rate might be larger than the pre-Cassini estimate, there are considerable differences between the continuum and stochastic models of the data. The continuum models are reliable below the exobase. However, it is not correct to use the standard expressions for thermal conduction above the exobase in order to power escape. In the stochastic models escape is caused by the molecular physics occurring in the thermosphere and corona. Although different conceptually, the resulting estimates of the mass loss rate could be consistent. That is, if atmosphere is being removed at the top, there must be an average upward flow *below* the exobase in order to replace the material removed (Tucker and Johnson 2009). At the temperatures and densities of interest heavy molecules can be removed at the top by any number of processes: formation and precipitation of larger molecules, ionospheric outflow, pick-up ion loss, atmospheric sputtering, photo-chemistry, viscous momentum transport from H₂, transport to another region of the atmosphere, or any combination of these processes.

Strobel (2008a, 2009) and Yelle et al. (2008) suggested that photon and plasma-induced hot recoils are not required. Rather upward thermal conduction of the solar energy deposited well below the exobase would produce a non-thermal tail in energy distribution of molecules in the exobase region, and that conduction would continue to act above the exobase to accelerate a fraction of the molecules to escape energies. Although the distorted Maxwellian extracted in Fig. 15.4a is consistent with this picture, such a spectrum led to *very small* escape fluxes. Therefore, these models require a considerable enhancement in the energetic tail for the flux of heavy molecules the size of which appears to be problematic (Johnson 2009; Tucker and Johnson 2009).

The upward flow of hydrogen molecules having thermal speeds much greater than that for the heavies (~ 1.2 km/s at 150 K) can, in principal, transfer momentum to the heavy molecules (e.g., Chamberlain and Hunten 1987). Cui et al. (2008) modeled the viscous energy loss to the heavy background molecules. In this model viscosity and heat conduction produces a Maxwellian speed distribution with an enhanced tail. But the viscous heating rate in Fig. 15.7 of Cui et al. (2008), ~ 2 eV/cm³/s, falls short of that required to drive the outflow of the heavy molecules. In fact, the modeling in Cui et al. (2008) requires that H₂ *draws energy from* the background gas, enhancing the tail of the H₂ velocity distribution function and reducing the likelihood of heavy molecule escape.

15.5.6 Monte Carlo Simulations: Tests of Continuum Models

Test particle simulations (e.g., Shematovich et al. 2003) and Direct Simulation Monte Carlo (DSMC) simulations have

been used to calculate the plasma-induced heating and escape at Titan (e.g., Michael et al. 2005a; Michael and Johnson 2005). These pre-Cassini results are given in Table 15.1 and Figs. 15.2 and 15.6. As mentioned earlier, the analytic model of atmospheric sputtering was tested by such simulations (Johnson 1994; Johnson et al. 2000) and was used in preliminary interpretations of Cassini INMS data in Titan's exobase region (DeLaHaye et al. 2007a).

Recently, DSMC simulations of the transition region have been carried out to test the slow hydrodynamic escape model for Titan (Tucker and Johnson 2009). Simulations of the transition region above 3900 km were carried out in 1D for both rectangular and spherical coordinates producing very similar results. The density and temperature at the lower boundary were normalized to that obtained in Strobel (2008a), Fig. 4) at 3900 km. That radial distance is well above the EUV and UV heating peaks. At an upper boundary 6200 km above the exobase, molecules were allowed to escape if they had energies greater than the escape energy, but were otherwise reflected allowing a more rapid approach to the steady state densities below 6200 km. Simulations were also carried out for an upper boundary at 8000 km showing a negligible effect on the resulting densities and temperatures. Although thermal conduction is correctly treated in the simulations, the atmosphere was found to be nearly isothermal, as seen in Fig. 15.8a, with essentially no escape. The numerical upper limit on the mass

loss rate for no heating above 3900 km and a pure N_2 atmosphere is $\sim 3 \times 10^{22}$ amu/s as compared to the $\sim (4-5) \times 10^{28}$ amu/s found in Strobel (2008a). Therefore, unlike the result in Fig. 15.7, when $\lambda_{\text{exo}} \sim 40$ at Titan's exobase and there is no external process causing an outflow, then no escape is expected beyond that estimated using Jean's escape.

The energy spectra of the molecules above the exobase were also examined and it was found that thermal conduction did not produce a noticeable enhanced tail (Tucker and Johnson 2009). However, when the molecules were *artificially removed* at the upper boundary of the simulations, as if by one of the loss processes discussed above (e.g., ionization and sweeping, knock-on collisions, etc.), then, not surprisingly, a decreasing temperature profile was obtained as seen in Fig. 15.8a.

Additional simulation of the exobase region and corona were carried out in which the Jeans parameter was reduced considerably in order to look for the onset of slow hydrodynamic escape. This was done by increasing the temperature at the lower boundary. Even for a Jeans parameter $\lambda_{\text{Jeans}} \sim 12$, in which the nitrogen corona becomes very extended, the actual loss rate was only about 1.5 times that of the Jeans rate calculated using the exobase temperature (Tucker and Johnson 2009).

Because CH_4 has a lower mass and is assumed to dominate the escape rate (Strobel 2008a, 2009; Yelle et al. 2008)), these simulations were then repeated for a mixed CH_4, N_2

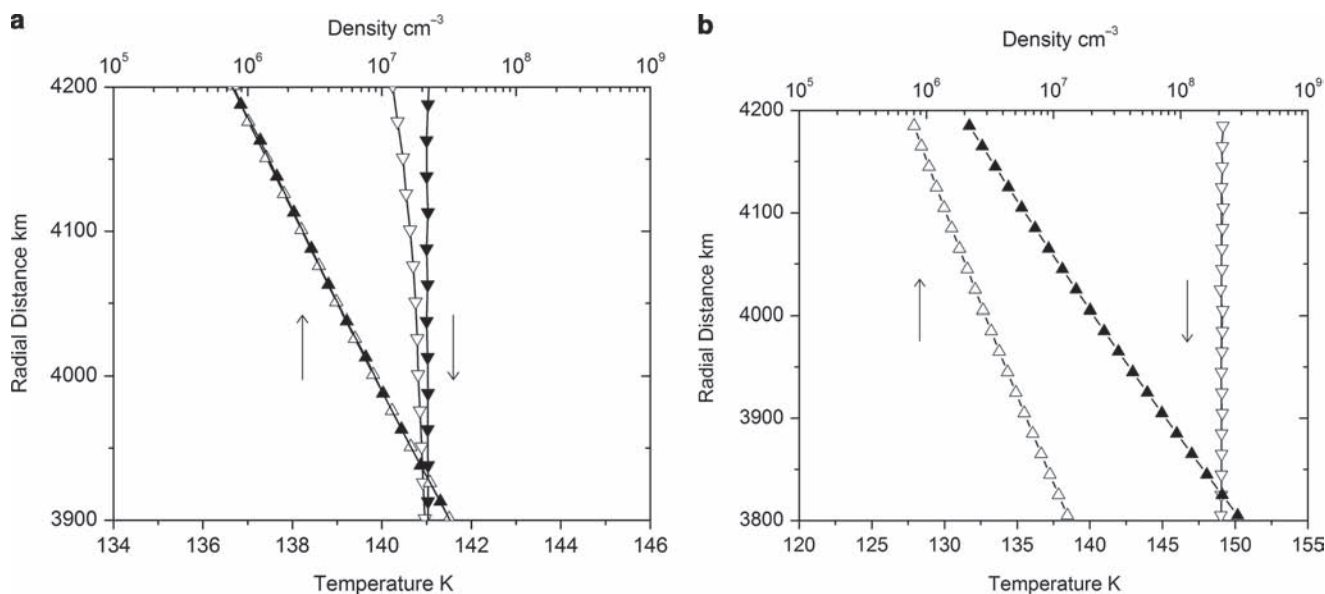


Fig. 15.8 Right panel: DSMC simulation of a nitrogen atmosphere: normalized at the lower boundary, 3800 km, to the density and temperature in Strobel (2008a) for his case of no heating above his lower boundary 3450 km. Density and temperature from two simulations are shown (Tucker and Johnson 2009); inverted triangles: no non-thermal escape process is included and T is found to be isothermal; in the second simulation molecular nitrogen is removed at the top boundary at a rate 4.5×10^{28} amu/s the escape rate proposed in (Strobel 2008a); the density changed

little over the radial distances shown but the temperature decreases consistent with adiabatic cooling. Results are for hard sphere cross sections which gave a slightly higher thermal conductivity than that in Strobel (2008a); similar results were obtained for forward directed cross sections (Tucker and Johnson 2009). Left panel: Density and temperature for $CH_4 + N_2$ atmosphere obtained from a DSMC simulation normalized to the mixing ratios temperature and densities in Yelle et al. (2008). Escape is again negligible and the temperature is essentially isothermal.

atmosphere. The lower boundary at 3775 km in these simulations had a mixing ratio, temperature and density normalized to that in Yelle et al (2008). Such simulations naturally allow for diffusive separation, thermal conduction and escape. Again the DSMC simulations *did not* result in escape and the atmosphere remained isothermal as seen in Fig. 15.8b. Such results suggest that it is unlikely that thermally-driven, slow hydrodynamic escape is occurring at Titan (Tucker and Johnson 2009).

15.6 Atmospheric Loss as Plasma and Plasma Heating: Cassini

MHD and hybrid simulations (Brecht et al. 2000; Ledvina et al. 2005; Ma et al. 2006; Sillanpaa et al. 2006) have shown that ions flow through the corona and exobase region and the fields penetrate below the exobase. Due to the plasma pressure in the ionosphere, ion outflow occurs (Wahlund et al. 2005; Coates et al. 2007) similar to that observed at Io (e.g., Wilson et al. 2002) and Venus (e.g., Terada et al. 2004). Estimates of the mass loss by ionospheric outflow have been made using Cassini data (Table 15.1). For T9 Sittler et al. (2009) directly measured the ionospheric loss down Titan's induced magnetotail with values $\sim 4 \times 10^6$ ions/cm²/s for mass 17 ions and $\sim 4 \times 10^6$ ions/cm²/s for mass 29 ions with field aligned flow speeds ~ 10 km/s and ion temperatures $T_{\text{ion}} \sim 4$ eV. Such ions contribute to the low energy peak in the heavy ion energy spectra in Fig. 15.6. The mass loss rates vary by an order of magnitude $\sim 0.1\text{--}4 \times 10^{26}$ amu/s. This is very roughly consistent with pre-Cassini estimates of the *neutral* loss rate, but smaller than the above loss rates. These estimates of the ion loss rate are obtained more directly than the neutral loss rates.

Ionospheric outflow, pick-up ions, and the influx of the slowed and deflected ambient ions can cause heating and neutral escape via ion-neutral momentum transfer and charge exchange collisions. The escape rates in Strobel (2008a) require $\sim 6 \times 10^8$ eV/cm²/s. This is comparable to the average energy flux extracted by DeLaHaye et al. (2007a) assuming the energy deposition rates in Table 15.2 occur over a scale height. However, this energy flux is larger than the $\sim 1 \times 10^8$ eV/cm²/s carried by the ion outflow above assuming it is global. Including the enhancement in the effective area of interaction due to the gyroradii of the heavy ions, which is about a factor of two (Hartle et al. 2006a, b; Shematovich et al. 2003), the energy flux *available* in the ambient plasma and fields is much larger, $\sim 2 \times 10^{10}$ eV/cm²/s (e.g., Johnson 2004). Although this indicates sufficient energy is available from the magnetosphere/ionosphere interaction, it is deposited over a broad range of altitudes. Therefore, molecular level modeling in the interaction

region combined with Cassini data will be required to describe the coupling and to calculate the plasma-induced escape rate. For instance, only a fraction of this energy flux contributes to the heating of the exobase by production of recoils as seen in Fig. 15.5 ($\sim 5 \times 10^9$ eV/cm²/s, Michael et al. 2005a; Michael and Johnson 2005). This flux was obtained from a hybrid model that had poor spatial resolution (~ 500 km) in the exobase region and produced loss rates well below the recent estimates. Therefore, the details of the plasma flow *and* the collisional coupling of the ions to the neutrals is critical. For instance, if the incident plasma has an energy spectrum such as that in Fig. 15.6, but the same energy flux used by Michael and Johnson (2005), that energy would be deposited in a much narrow region about the exobase, as seen in Fig. 15.5, so that the required energy densities could easily be achieved.

Details of the energy deposition are given in the Chapter 16. Those authors note that the observed influx of keV oxygen ions from the magnetosphere. $\sim 0.9 \times 10^{24}$ O⁺ ions/s impact Titan's atmosphere and corona (Hartle et al. 2006a, b), is consistent with the observation of oxygen chemistry in Titan's upper atmosphere (Hörst et al. 2008). Using a mean ion energy of \sim keV, one gets an energy flux $\sim 5.0 \times 10^8$ eV/cm²/s at exobase heights. This is fortuitously close to the maximum plasma heating rate allowed by Strobel (2009) resulting in an energy deposition rate comparable to the above estimates, so the O⁺ could contribute a significant fraction of the required plasma energy flux.

Sillanpaa et al. (2007) find $\sim 10^{24}$ O⁺/s are lost to interactions with Titan, depositing a globally averaged energy flux $\sim 10^9$ eV/cm²/s normalized to the *exobase surface*. Estimates of the energy deposition rates by the *incoming ions* using hybrid and MHD models (Brecht et al. 2000; Ledvina et al. 2005; Sillanpaa et al. 2007) are below the rates extracted by DeLaHaye et al. (2007a). In such simulations, the ion energy deposition rate into the atmosphere is sensitive to the fields penetrating the exobase region. Therefore, modeling the ion and energetic neutral flow through the exobase region and their collisional coupling to the background neutrals is critical. For instance, ions and energetic neutrals penetrating the corona (Michael et al. 2005a), pick-up ions formed close to the exobase, and ions out-flowing from the ionosphere follow the field lines. Therefore, they not only penetrate the exobase but can cross the exobase from below. The momentum transfer from exiting ions to neutrals considerably enhances the effective sputtering efficiency and is often referred to as forward sputtering (Johnson 1990, 1994). In this way the ionospheric outflow can collisionally drag out neutrals.

Based on CAPS data (e.g., Fig. 6 and Coates et al. 2007) and data from other instruments (e.g., Wahlund et al. 2005; Sittler et al. 2008), there is a flux of low energy ions flowing through the corona that has not been incorporated into

the simulations. There is also a flux of very energetic ions ($\gg 10$ keV) (Ledvina et al. 2005), but these deposit their energy at depths well below the exobase (e.g., Luna et al. 2003; Cravens et al. 2008) and do not affect escape. If atmospheric sputtering is the dominant process driving escape, which is not at all clear, it is the low energy heavy pick-up and ionospheric ions that need to be included in new simulations of Titan's exobase region. Fortunately, more detailed models of the plasma flow through the exobase region, constrained by Cassini plasma data, are now becoming available.

Based on density vs altitude profiles, such as those in Fig. 15.3b, it has been suggested that a non-thermal energizing process is occurring in the exobase region (DeLaHaye et al. 2007a). Therefore, effective scale heights for the mass density vs altitude are shown in Fig. 15.9 for a number of exobase crossings. Although there is considerable variability, possibly due to Titan's position in Saturn's plasma sheet (Chapter 16), with one exception the steepest profiles, suggestive of the highest temperatures and/or highest escape rates, are associated with the combined plasma/solar flux directions. Whereas the coronal structure can respond promptly to changes in the incident flux, time lags and horizontal transport affect the exobase structure (Muller-Wodarg et al. 2008). The full suite of the atmospheric density profiles is now being compared to the plasma flow data from the CAPS and MIMI instruments.

15.7 Titan Mass Loss: Magnetospheric Implications

Titan atmospheric mass loss is also of interest as a source of neutrals and plasma for Saturn's magnetosphere. Therefore, the composition of the ambient plasma near Titan's orbit can be used to test the atmospheric loss rate. Prior to the arrival of Cassini, hydrogen from Titan was thought to be the dominant neutral source to the magnetosphere. Although smaller mass loss rates were estimated for heavy species, Titan was still assumed to be an important, and possibly dominant, source of nitrogen for the magnetosphere. Since the present escape rates are unsettled, new models for the Titan heavy molecules tori are not yet available. Figure 15.10 shows the spatial distribution based on pre-Cassini estimates of the atmospheric sputtering rates for the nitrogen component. Based on recent estimates for the source rate, the densities shown would be far too low, but the morphology for comparable masses will be similar and the neutral densities would roughly scale by the loss rate. It was anticipated that Cassini should be able to observe pick-up ions from a neutral torus even with densities as low as those predicted in Fig. 15.10, however, such ions have not been observed.

The sources of neutrals for Saturn's magnetospheric are given in Table 15.2. Titan does not appear to be the dominant source of nitrogen (e.g., Smith et al. 2005, 2007, 2008) and is not the dominant source of mass for Saturn's magnetosphere

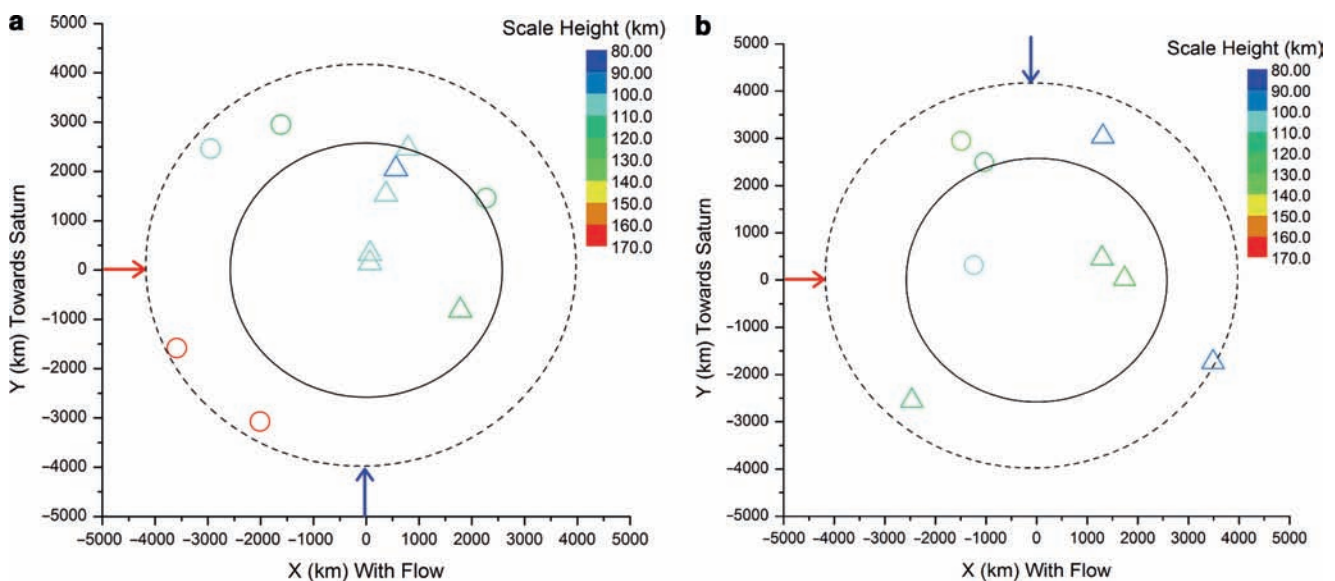


Fig. 15.9 North polar view of Titan showing the scale height in the corona vs Titan's orbital position and the position of the exobase crossing in Titan's atmosphere. Scale heights obtained from fits to the INMS data from 1500 to 2000 km (colored triangles and circles) represent ingress and egress points respectively: (a) crossings for times periods 9 am–3 pm Saturn local time (Titan on the dayside of Saturn); (b) from 9 pm to 3 am Saturn local time (Titan on the nightside of Saturn). Red

are the steepest profiles (largest scale height) and blue are the least steep (smallest scale height). Arrows indicate directions of the external energy flux: blue, solar; red plasma: the co-rotating plasma flow which is, of course, significantly altered close to the exobase: e.g. (Sillanpaa et al. 2007) and a correlation with the actual plasma flux is needed. Solid circle indicate Titan's surface, and dashed circle indicates an exobase at 1500 km in the z plane.

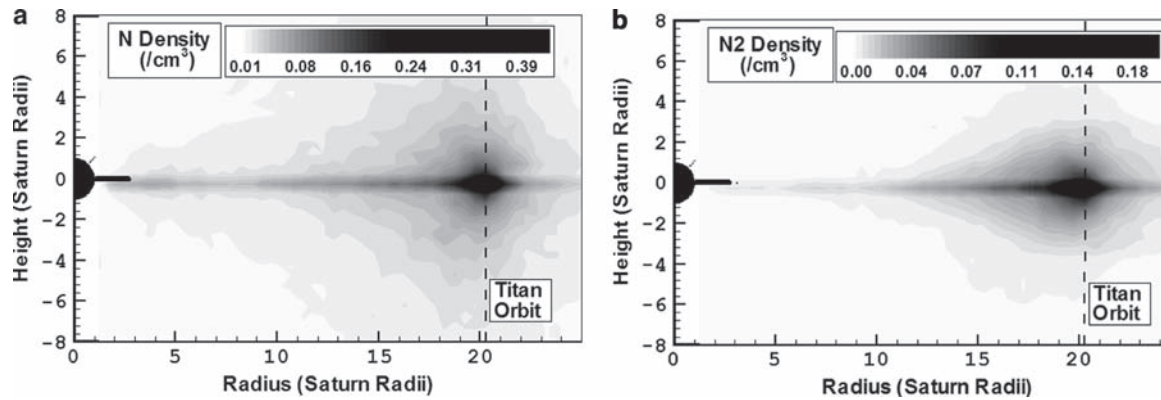


Fig. 15.10 Map of the spatial distribution of mass 14 and mass 28 (Smith et al. 2004): based on pre-Cassini estimates of the atmospheric loss rates from photochemistry (Shematovich et al. 2003) and sputtering Michael et al. 2005a): Mass 28 ($\sim 1.7 \times 10^{26}$ amu/s) and Mass 14

($4.5 \times 10^{26} \text{ s}^{-1}$) from a Titan nitrogen atmosphere ($\sim 6 \times 10^{26}$ amu/s). These profiles scale roughly linearly with the source rate and, therefore can be used along with more recent estimates of the loss rates.

even for the largest proposed escape rates as seen in Table 15.2. However, if the largest methane source rate ($\sim 4\text{--}5 \times 10^{28}$ amu/s: Yelle et al. 2008; Strobel 2008a) is correct, then Titan could be the dominant source of carbon for the magnetosphere. However, Cassini measurements suggest that this is not the case.

Source	Source rate (10^{29} amu/s)	Composition ^a
Rings ^b	~ 6	O_2, H_2
Enceladus ^c	$\sim 1\text{--}4$	H_2O ($\sim 4\%$ C or N species)
Titan ^d	0.03- 0.5	$\text{N}_2, \text{CH}_4, \text{H}_2$

^aMolecular dissociation products would also be present for all of these species.

^bJohnson et al. 2006b.

^cJohnson et al. 2006a; Melin et al. 2009; Hansen et al. 2006; Waite et al. 2006.

^dDeLaHaye et al. 2007a (N_2, CH_4); Cui et al. 2008 (H_2); Strobel 2008a (CH_4, H_2); Yelle et al. 2008 (CH_4).

Since neutrals ejected from Titan continue to orbit Saturn until they are ionized, they can be detected indirectly by measuring the ambient plasma composition. Detection of Titan-generated particles is possible not only close to Titan's orbit, but over a broad region of Saturn's magnetosphere (Smith et al. 2004). Although the neutrals converted to ions close to Titan or in its wake are rapidly lost down the magnetotail or in an injection event, a background plasma has been detected in the vicinity of Titan's orbit. Outward diffusion of ions produced closer to Saturn can contribute to this plasma, but such ions are also lost prior to crossing Titan's orbit. In addition, they tend to adiabatically cool which would result in cold plasma that is not observed. Consequently, the measured phase space distributions of detected ions indicate that the ambient plasma near Titan's orbit is dominated by neutrals ionized in the outer magnetosphere (Szego et al. 2005; Sittler et al. 2006). Since any oxygen ionized in this

region must be scattered to the outer magnetosphere from the Enceladus and OH tori (Johnson et al. 2006a) or from the ring atmosphere (Johnson et al. 2006b), carbon containing ions should dominate oxygen ions near Titan's orbit if the largest methane loss rates are correct.

However, the plasma upstream from Titan has been shown to contain a substantial fraction of O^+ (Hartle et al. 200a, b). The ratio of oxygen to carbon containing ions for SOI was estimated to be ~ 1.5 (Hartle et al. 2006b). Scaling the suggested loss rates to earlier models of the neutral density from all sources (e.g., Johnson et al. 2006a, b; Smith et al. 2004, 2005, 2007), such an ion fraction is much larger than would be predicted by the highest methane source rate. Determining the present carbon loss rate from ion density measurements in the magnetosphere will require a good model of the oxygen and carbon neutral densities and ionization rates near Titan's orbit. In addition, the carbon and oxygen fractions in the ambient plasma will have to be measured for a variety of plasma conditions.

15.8 Summary

Based on Cassini data for many passes through Titan's upper atmosphere, knowledge of the thermospheric structure and its interaction of Saturn's magnetosphere are rapidly improving. Therefore, it is exciting that kinetic modeling of the present escape mechanisms, constrained by in situ data, is now possible. In this way, the differences in the loss mechanisms proposed will be resolved. However, because of the observed variability in the nature of the interaction, it is likely that analysis of the data from many passes through the thermosphere and corona will be required to unravel the atmospheric escape processes.

Although the calculated hydrogen loss rate ($\sim 0.8\text{--}2 \times 10^{28}$ amu/s; Cui et al. 2008; Bell et al. 2009) is similar to the pre-Cassini estimate, considerable enhancements in the loss of heavy molecules have been suggested: $\sim 0.3\text{--}4 \times 10^{28}$ amu/s. If the largest loss rates for the heavy species persisted for ~ 4 Gyr, the net mass loss would be of the order of the present atmospheric mass. In addition, if such loss rates were primarily CH_4 , then the present CH_4 inventory would be lost in $<10^8$ years. This rate is about an order of magnitude smaller than the principal atmospheric mass loss process, loss of methane by precipitation of hydrocarbons. However, it can have a significant affect on modeling the evolution of Titan's atmosphere (Chapters 7 and 8). For this reason accurately understanding the mechanisms driving escape (e.g., Johnson et al. 2008) is critical. The estimates of the escape rate in DeLaHaye et al (2007a) were poorly constrained since the density data covered a narrow range of altitudes in the corona. If the kappa distributions they extracted for the molecular energy spectra at the exobase are correct for describing the corona structure at all altitudes, then the heavy molecule escape rate is small, consistent with pre-Cassini estimates. Their *preferred escape rate*, obtained by scaling the extracted energy deposition rate to simulations and averaged over five passes, showed a larger heavy molecule escape rate ($\sim 0.3 \times 10^{28}$ amu/s), but one that is much smaller than the upward flows extracted by Yelle et al. (2008), Muller-Wodarg et al. (2008) and Strobel (2008a, 2009). *However, the average upper limit* in DeLaHaye et al. (2007a), obtained using a model recoil spectrum, allowed for large escape rates. If these upper limits are correct, then a 1D analysis of the density data below the exobase would result in an upward flow such as that found in the continuum models. In that case, the three mass loss rates would be roughly consistent, although the mechanisms proposed are very different.

Although there is evidence, such as that in Fig. 15.2b, for large extensions of the corona and, possibly, concomitant large local escape rates, the lower *average* escape rates are more likely. Therefore, the continuum models likely need re-examination including both the diffusive replacement of the precipitating carbon and accurate descriptions of the transition region. In addition, good estimates of the amount and spatial distribution of the plasma-induced energy flux is required. Although, the plasma energy deposition rate in the exobase region is larger than the average EUV heating rate, an even larger plasma heating rate or more efficient coupling of the plasma to the neutrals than that in Michael et al. (2005a) would be required to obtain the largest suggested escape rates.

If the largest estimate for the upward flow of heavy molecules at the exobase is correct, but the plasma heating is inadequate to drive escape, then one of the following must be true: another non-thermal process must be active; the upward flow in the regions studied indicates transport of mass to another

region of the atmosphere; the upward diffusive flux of methane is due to replacement of the methane lost by precipitation; or heat from below acts to drive escape as proposed by Yelle et al. (2008) and Strobel (2008a). However, preliminary DSMC simulations do not support the thermal conduction mechanism for the loss of carbon and nitrogen, nor does the ion composition in the ambient plasma appear to agree with the methane mass loss rates in Yelle et al (2008) and Strobel (2009). Therefore, additional molecular simulations, constrained by Cassini data, are needed and as well as a description of the morphology of the transport of material in the corona.

A detailed understanding of the present atmospheric escape rate is a precondition for understanding the origin and evolution of Titan's atmosphere and its astrobiological potential (Chapters 7–9). Therefore, it is exciting that the concepts for mass loss from Titan's atmosphere and plasma-induced heating can now be re-examined based on a wealth of Cassini data

Acknowledgements We acknowledge comments by T. Cassidy, I. Sillanpaa, J. Bell, J. Westlake, and B. Magee. Work at U. Virginia, GSFC and SwRI is supported by the Cassini Program under JPL Contract 1243218 with SwRI. Additional support at U. Virginia is provided by NASA's Cassini Data Analysis Program and NASA's Planetary Atmospheres Program.

References

- Barbosa DD (1987) Titan's atomic nitrogen torus: inferred properties and consequences for the Saturnian Aurora. *Icarus* 72:53–61
- Bell JM, Bougher SW, Waite JH Jr, Ridley AJ, Magee B, Bar-Nun A, Toth G, De La Haye V (2009) Simulating the global mean structure of Titan's upper atmosphere using the titan global ionosphere-thermosphere model. *Planet Space Sci* (in press)
- Bertucci C; plus 11 (2008) The magnetic memory of titan's ionized atmosphere science 321:1475–1477
- Bird GA (1994) DSMC procedures in a homogenous gas. In: *Molecular gas dynamics and the direct simulation of gas flows*. Clarendon, Oxford, UK, pp 218–256
- Brecht SH, Luhmann JG, Larson DJ (2000) Simulation of the Saturnian magnetospheric interaction with Titan. *J Geophys Res* 105:13119–13130
- Chamberlain JW, Hunten D (1987) *Theory of Planetary Atmosphere*. Academic, New York
- Coates AJ, Crary FJ, Young DT, Szego K, Arridge CS, Bebesi Z, Sittler EC Jr, Hartle RE 4, Hill TW (2007) *Geophys Res Lett* 34:L24S05. doi:10.1029/2007GL030919
- Cravens TE, Keller CN, Ray B (1997) Photochemical sources of non-thermal neutrals for the exosphere of Titan. *Planet Space Sci* 45: 889–896
- Cravens TE, Robertson IP, Ledvina SA, Mitchell D, Krimigis SM, Waite JH (2008) *Geophys Res Lett* 35. doi: 10.1029/2007GL032451
- Cui J, Yelle RV, Volk K (2008) Distribution and escape of molecular hydrogen in Titan's thermosphere and exosphere. *J Geophys Res* 113. doi:10.1029/2007JE003032

- De La Haye V, Waite JH Jr, Cravens TE, Nagy AF, Yelle RV, Johnson RE, Lebonnois S, Robertson IP (2007b) Titan's carona: the contribution of exothermic chemistry. *Icarus* 191:236–250
- DeLaHaye V, Waite JH Jr, Johnson RE et al. (2007a) Cassini ion and neutral mass spectrometer data in Titan's upper atmosphere and exosphere: observation of a suprathermal corona. *J Geophys Res* 112:A07309. doi:10.1029/2006JA0122
- Fulchignoni M, Ferri F, Angrilliet F et al (2005) Titan's physical characteristics measured by the Huygens Atmospheric Structure Instrument (HASI). *Nature* 438:785–791
- Garnier P, Dandouras I, Toubanc D, Brandt PC, Roelof EC, Mitchell DG, Krimigis SM, Krupp N, Hamilton DC, Waite H (2007) The exosphere of Titan and its interaction with the kronian magnetosphere: MIMI observations and modeling. *Planetary and Space Science* 55:165–173
- Garnier P, Dandouras I, Toubanc D, Roelof EC, Brandt PC, Mitchell DG, Krimigis SM, Krupp N, Hamilton DC, Dutuit O, Wahlund J-E (2008) The lower exosphere of Titan: Energetic neutral atoms absorption and imaging. *J Geophys Res* 113, doi:10.1029/2008JA013029
- Gustin J, Ajello JM, Stevens MH, Stephan AW, Stewart I, Larsen K, Esposito L, McClintock W (2009) Titan airglow spectra from Cassini UVIS: III. FUV Limb Analysis. *Geophys Res Lett* (in press)
- Hansen CJ, Esposito L, Stewart AIF, Colwell J, Hendrix A, Pryor W, Shemansky D, West R (2006) Enceladus' water vapor plume. *Science* 311:1422–1425
- Hartle RE, 17 authors (2006a) Preliminary interpretation of Titan plasma interaction as observed by the Cassini Plasma Spectrometer: comparisons with Voyager 1. *Geophys Res Lett* 33:L08201. doi:10.1029/2005GL024817
- Hartle RE, 17 authors (2006b) Initial interpretation of Titan plasma interaction as observed by the Cassini plasma spectrometer: comparisons with Voyager 1. *Planet Space Sci* 54:1211–1224
- Hartle RE, Sittler EC, Ogilvie KW, Scudder JD, Lazarus AJ, Atreya SK (1982) Titan's ion exosphere observed from Voyager 1. *J Geophys Res* 87:1383–1394
- Hirschfelder JO, Curtiss CF, Bird RB (1964) *Molecular theory of gases and liquids*. Wiley, New York, 2nd corrected printing
- Hörst SM, Vuitton V, Yelle RV (2008) Origin of oxygen species in Titan's atmosphere. *J Geophys Res* 113, doi:10.1029/2008JE003135
- Johnson RE (1990) *Energetic charged-particle interactions with atmospheres and surfaces*, Springer, Berlin
- Johnson RE (1994) Plasma-induced Sputtering of an Atmosphere. *Space Sci Rev* 69:215–253
- Johnson RE (2004) The magnetospheric-plasma-driven evolution of satellite atmospheres. *Astrophys J* 609:L99–L102
- Johnson RE (2009) Plasma-induced heating and escape. *Proc. Royal Soc (London)* 367:753–771. doi:10.1098/rsta.2008.0244
- Johnson RE, Schnellenberger D, Wong MC (2000) The sputtering of an oxygen thermosphere by energetic O. *J Geophys Res* 105:1659–1670
- Johnson RE, Smith HT, Tucker OJ, Liu M, Tokar R (2006a) The Enceladus and OH Tori at Saturn. *Astrophys J Lett* 644:L137–L139
- Johnson RE, Luhmann JG, Tokar RL, Bouhram M, Berthelier JJ, Sittler EC, Cooper JF, Hill TW, Smith HT, Michael M, Liu M, Crary FJ, Young DT (2006b) Production, ionization and redistribution of O₂ Saturn's ring atmosphere. *Icarus* 180:39
- Johnson RE, Combi MR, Fox JL, Ip W-H, Leblanc F, McGrath MA, Shematovich VI, Strobel DF, Waite JH Jr (2008) Exospheres and Atmospheric Escape. *Space Sci Rev* 139:355–397
- Jurac S, McGrath MA, Johnson RE, Richardson JD, Vasyliunas VM, Eviatar A (2002) *Geophys Res Lett* 29. doi:10.1029/2002GL015855
- Krasnopolsky VA (1999) Hydrodynamic flow from Pluto. *J Geophys Res* 104:5955–5962
- Krestyanikova MA, Shematovich VI (2006) Stochastic models of hot planetary and satellite coronas: a hot oxygen corona of Mars. *Solar Sys Res* 40:384–392
- Lammer H, Bauer SJ (1993) Atmospheric mass loss from Titan by sputtering. *Planet Space Sci* 41:657–663
- Lammer H, Stumptner W, Bauer SJ (1998) Dynamic escape of H from Titan as a consequence of sputtering induced heating. *Planet Space Sci* 46:1207–1213
- Lammer H, Kasting JF, Chassefière E, Johnson V, Kulikov YN, Tian YN (2008) Atmospheric escape and evolution of terrestrial planets and satellites. *Space Sci Rev*, *Space Sci Rev* 139:399–436. doi 10.1007/s11214-008-9413-5
- Leblanc F, Johnson RE (2001) Sputtering of the Martian atmosphere by solar wind pick-up ions. *Planet Space Sci* 49:645–656
- Leblanc F, Johnson RE (2002) Role of molecular species in pickup Ion sputtering of the Martian atmosphere. *J Geophys Res* 107:5-1–5-6. doi:10.1029/2000JE001473
- Lebonnois S, Bakes ELO, McKay CP (2003) Atomic and molecular hydrogen budget in Titan's atmosphere. *Icarus* 161:474–485
- Ledvina SA, Cravens TE, Kecskemety K (2005) Ion distributions in Saturn's magnetosphere near Titan. *J Geophys Res* 110. doi:10.1029/2004JA010771
- Luna H, Michael M, Shah MB, Johnson RE, Latimer CJ, McConkey JW (2003) Dissociation of N₂ in capture and ionization collisions with fast H⁺ and N⁺ ions and modeling of positive ion formation in the Titan atmosphere. *J Geophys Res* 108. Doi:10.1029/2002JE001950
- Ma Y, Nagy AF, Cravens TE, I Sokolov V, Hansen KC, Wahlund J-E, Crary FJ, Coates AJ, Dougherty MK (2006) Comparisons between MHD model calculations and observations of Cassini flybys of Titan. *J Geophys Res* 111. doi:10.1029/2005JA011481
- Ma Y-J, Altwegg K, Breus T, Combi MR, Cravens TE, Kallio E, Ledvina SA, Luhmann JG, Miller S, Nagy AF, Ridley AJ, Strobel DF (2008) Plasma flow and related phenomena in planetary aeronomy. *Space Sci Rev* 139:311–353
- Magee B, et Waite JH, Bell KM, Westlake JM, Gell J, De La Haye V (2009) INMS Derived Composition of Titan's Upper Atmosphere: Analysis Methods and Model Comparisons. *Planet.Space Sci.* (in press) doi:10.1016/j.pss.2009.06.016
- Mandt KE, Waite JH Jr, Lunine JJ, Magee BA (2009) Isotopic evolution of Titan's main constituents. *Planet Space Sci*, in press doi:10.1016/j.pss.2009.06.005
- Marconi ML, Dagum L, Smyth WH (1996) Hybrid fluid mechanic/kinetic theory approach to planetary atmospheres: an example of an intermediate mass body. *Astrophys J* 469:393–401
- McNutt RL (1989) Models of Pluto's upper atmosphere. *Geophys Res Lett* 16:1225–1228
- Melin H, Shemansky DE, Liu X (2009) The distribution of hydrogen and atomic oxygen in the magnetosphere of Saturn. *Icarus* in press
- Michael M, Johnson RE (2005) Energy deposition of pickup ions and heating of Titan's atmosphere. *Planet Space Sci* 53:1510–1514
- Michael M, Johnson RE, Leblanc F, Liu M, Luhmann JG, Shematovich VI (2005a) Ejection of nitrogen from Titan's atmosphere by magnetospheric ions and pick-up ions. *Icarus* 175:263–267
- Michael M, Johnson RE, Leblanc F, Smith HT, Berthelier JJ, Bouhram M, Chassefière E, Sittler EC, Hartle RE, Coates AJ, Hill TW, Young DT (2005b) Atmospheric sputtering and heating, Spring 2005 Crete Titan/Cassini-Huygens meeting. Crete, Greece
- Mitchell DG, Brandt PC, Roelof EC, Dandouras J, Krimigis SM, Mauk BH (2005) Energetic neutral atom emissions from Titan interaction with Saturn's magnetosphere. *Science* 308:989–992
- Muller-Wodarg ICF, Yelle RV, Borggren N, Waite JH Jr (2006) Waves and horizontal structures in Titan's thermosphere. *J Geophys Res* 111, doi:10.1029/2006JA011961
- Muller-Wodarg ICF, Yelle RV, Cui J, Waite JH Jr (2008) Horizontal structures and dynamics of Titan's thermosphere. *J Geophys Res* 113, CiteID E10005 10.1029/2007JE003033
- Nagy AF, Cravens TE, Yee J-H, Stewart AIF (1981) Hot oxygen atoms in the upper atmosphere of Venus. *Geophys Res Lett* 8(June):629–632

- Penz T, Lammer H, Kulikov YuN, Biernat HK (2005) The influence of the solar particle and radiation environment on Titan's atmosphere evolution. *Adv Sp. Res* 36:241–250
- Schunk RW (1975) Transport equations for aeronomy. *Planet Space Sci* 23:437–485
- Schunk RW, Nagy AF (2000) Ionospheres: physics, plasma physics, and chemistry. In: Dressler AJ, Houghton JT, Rycroft MJ (eds) *Cambridge Atmo Space Sc. Ser.* Cambridge University Press, Cambridge, UK, pp 104–147
- Shematovich VI, Johnson RE, Michael M, Luhmann JG (2003) Nitrogen loss from Titan. *J Geophys Res* 108(E8):5087. doi:10.1029/003JE002094
- Sigmund P (1981) Sputtering by particle bombardment: theoretical concepts. In: Behrisch R (ed) *Sputtering by Particle Bombardment I*, Springer, Berlin, pp 9–67
- Sillanpaa I, Kallio E, Janhunen P, Schmidt W, Mursula K, Vilppola J, Tanskanen P (2006) Hybrid simulation study of ion escape at Titan for different orbital positions. *Adv Space Res* 38:799–805
- Sillanpaa I, Kallio E, Jarvinen R, Janhunen P (2007) Oxygen ions at Titan's exobase in a Voyager 1 – type interaction from a hybrid simulation *J Geophys Res* 112. doi:10.1029/2007JA012348, 2
- Sittler EC, Thomson M, Johnson RE et al. (2007) Cassini observations of Saturn's inner plasmasphere: Saturn orbit insertion result. *Planet Space Sci* 54:1197–1210 (2006). Erratum: *Planet Space Sci* 55:2218–2220
- Sittler EC et al. (2006) Energetic nitrogen ions within the inner magnetosphere of Saturn. *J Geophys Res* 111:A09223, doi:10.1029/2004JA010509
- Sittler EC et al. (2008) Ion and neutral sources and sinks within Saturn's inner magnetosphere Cassini results: *Planet Space Sci* 56:3–18
- Sittler EC et al. (2009) Composition of upstream flow for Titan's interaction with Saturn's magnetosphere: preliminary results. *Planet Space Sci* (in press)
- Smith HT, Johnson RE, Shematovich VI (2004) Titan's atomic and molecular nitrogen tori 3. *Geophys Res Lett* 31:L16804. doi:10.1029/2004GL020580
- Smith HT, Shappirio M, Sittler EC, Reisenfeld D, Johnson RE, Baragiola RA, Cray FJ, McComas DJ, Young DT (2005) Discovery of nitrogen in Saturn's inner magnetosphere. *GRL* 32:L14S03. doi:10.1029/2005GL022654
- Smith HT, Johnson RE, Sittler EC, Shappirio M, Tucker OJ, Burger M, Cray FJ, McComas DJ, Young DT (2007) Enceladus The likely dominant nitrogen source in Saturn's magnetosphere. *Icarus* 188:356–366
- Smith HT, Shappirio M, Johnson RE, Reisenfeld D, Sittler EC, Cray FJ, McComas DJ, Young DT (2008) Enceladus: A potential source of ammonia products and molecular nitrogen for Saturn's magnetosphere. *J Geophys Res* doi:10.1029/2008JA013352.
- Smith HT, Mitchell DG, Johnson RE, Paranicas C (2009) Investigation of energetic proton penetration in Titan's atmosphere using the Cassini INCA instrument. *Planet Space Sci* doi:10.1016/j.pss.2009.03.013.
- Strobel DF (2002) Aeronomic Systems on Planets, Moons, and Comets. In: Mendillo M, Nagy A, Waite H (eds) *Comparative Aeronomy in the Solar System*, American Geophysical Union, *Geophysical Monograph Series*, pp 7–22
- Strobel DF (2008a) Titan's hydrodynamically escaping atmosphere. *Icarus* 193:588–594
- Strobel DF (2008b) N₂ escape rates from Pluto's atmosphere. *Icarus* 193:612–619
- Strobel DF (2009) Titan's hydrodynamically escaping atmosphere: escape rates and the structure of the exobase region. *Icarus* 202:632–641
- Strobel DF, Shemansky DE (1982) EUV emissions from Titan's upper atmosphere: Voyager I encounter. *J Geophys Res* 87:1361–1368
- Szego K et al. (2005) The global plasma environment of Titan as observed by Cassini Plasma Spectrometer during the first two close encounters with Titan. *Geophys Res Lett* 32:L20S05. doi:10.1029/2005GL022646
- Terada N, Shinagawa H, Machida S (2004) Global hybrid model of the solar wind interaction with the Venus ionosphere: ion escape processes. *Adv Space Res* 33:161–166
- Tucker OJ, Johnson RE (2009). Thermally driven atmospheric escape: Monte Carlo simulations for Titan's atmosphere. *Planet Space Sci* 11 June doi:10.1016/j.pss.2009.06.003
- Vasyliunas VM (1968) A survey of low-energy electrons in the evening sector of the magnetosphere with OGO 1 and OGO 3. *J Geophys Res* 73:2839–2885
- Wahlund J-E, 17 coauthors (2005) Cassini measurements of cold plasma in the ionosphere of Titan. *Science* 308:982–986
- Waite JH Jr, 13 authors (2006) Cassini ion and neutral mass spectrometer: Enceladus plume composition and structure. *Science* 311(5766): 1419–1422
- Waite JH Jr, 21 authors (2005) Ion neutral mass spectrometer results from the first flyby of Titan. *Science* 308:982–986
- Wei HY, Russell CT, Wahlund J-E, Dougherty MK, Bertucci C, Modolo R, Ma YJ, Neubauer FM (2007) Cold ionospheric plasma in Titan's magnetotail. *Geophys Res Lett* 34:CiteID L24S06. doi:10.1029/2007GL030701
- Wilson EH, Atreya SK (2004) Current state of modeling the photochemistry of Titan's mutually dependent atmosphere and ionosphere. *J Geophys Res* 109. doi:10.1029/2003JE002181
- Wilson JK, Mendillo M, Baumgardner J, Schneider NM, Trauger JT, Flynn B (2002) The dual sources of Io's sodium clouds. *Icarus* 157:476–489
- Yelle RV, Cui J, Muller-Wodarg ICF (2008) Methane escape from Titan's atmosphere. *J Geophys Res* 113. doi:10.1029/2007JE003031